POLITECNICO DI TORINO

Facoltà di Ingegneria

Master's degree course in Electronic Engineering

Master's Degree Thesis

Study of a low-power remote sensor node based on LoRa

Supervisor
Prof.ssa Patrizia Savi

Candidate
Alessandro Berruti

Internship Tutor
Ing. Mirko Zanotel

Anno accademico 2017-2018

Contents

Summary

Overview and scope of the thesis

The future energy market will be characterized by an increasing need of monitoring and using energy differently in order to both reduce consumption and change the user habits providing new commercial offers that will be more and more tailored.

In the last years a lot of business solutions have been proposed by energy suppliers to make the user (and themselves) constantly aware of the energy consumed, providing some commercial kits that can include other type of domotic devices, like door/window alarms, gas and water sensors, remote controlled sockets and so on. These solutions often cover typical user needs, but they offer a limited user experience and low performance for the energy monitoring.

This thesis work takes part in a IoT project that encompasses an innovative smart metering solution for the monitoring of power drawn and energy consumption in domestic and small business environments. Information related to the energy/power measurements are generated by a sensor that is installed in proximity of the energy meter and detect consumption by measuring the pulses of the meter LED. The sensor sends consumption data to a gateway that manages this information updating both a smart HMI and a cloud server.

The sensor is the most critical part of this system because of a series of constraints and performance requirements requested in the project. The most important constraint is the use of wireless communication due to the need to avoid any intervention on the electric plant or professional installation in the related premises. Since the energy meter is usually placed in a deep-indoor location (basement, box, etc.), the sensor can hardly communicate with the gateway that is installed far away and in a different place. The other constraint is the sensor battery supply that must last at least 3 years without recharging.

The objective of this thesis is to find the better solution for this sensor in terms of RF technology, protocol and battery size that maximize the transmission rate and achieve the requested battery life.

This result has been achieved studying, modeling and optimizing the point-to-point link between the sensor and the gateway and maximizing the sensor node

battery life.

Workflow and Results

Since RF communication and easy installation were the main constraints for the sensor, a research of different available wireless technologies has been conduced. LoRa has been selected since it ensures an high immunity and receiver sensibility, whereas other technologies has been considered not suitable for they lower performances and their need of a more complex network.

To validate this choice, some tests have been performed using different buildings and environments. The results have shown some critical issues related to the building structure and gave us the possibility to understand the effect of different parameters setting of the LoRA transceiver on the indoor propagation. Even if LoRa have an high concrete penetration capability, its radio setting is subject to a trade-off between range, transmission time and energy used.

A study of the sensor energy management has been performed as well, analyzing the efficiency of the power amplifiers and how different RF parameters settings and mismatch of the antenna affect battery consumption. An additionally study has been conduced on different methods and devices used to determine the discharge and the state of charge of the primary lithium battery.

The final point was the implementation of a model that simulates the network with different transmission strategies. This model was first developed with *Matlab/Simulink* and then redesigned with *SystemC* to speed up simulation and to allow the sensor's firmware integration into the model. The model was fed with realistic data of energy consumption that were acquired from some energy meters using a special device that was properly developed for this purpose. With simulation it was possible to evaluate the effect of different combination of RF parameters and communication strategies on latency and battery discharge, avoiding long tests and debug sessions on the field.

The final result has been a software strategy that is able to reduce the number of transmissions without modifying the user experience and providing a good representation of user consumption profile. With a proper configuration of this strategy the requested battery life of about 3 years can be achieved.

This work lays the basis for further studies of IoT networks involving other types of battery powered sensors and give the possibility to study the network scalability with more accurate and complex models.

List of Figures

List of Tables

Glossary

3GPP 3rd Generation Partnership Project. 14

ADC Analog to Digital Converter. 33

AFA Adaptive Frequency Agility. 18

AWGN Additive White Gaussian Noise. 21

BLE Bluetooth Low Energy. 6, 7

BPSK Binary Phase Shift Keying. 7, 9

BT Bluetooth. 6, 7

BW Bandwidth. 24

CAD Channel Activity Detection. 18

CEPT/ECC Electronic Communications Committee. 16

CR Coding Rate. 25

CRC Cyclic Redundancy Check. 24

DSSS Direct Sequence Spread Spectrum. 3, 5, 7, 21, 22

DUT Device Under Test. 16, 17, 52

EC European Commission. 16

EDGE Enhanced Data rates for GSM Evolution. 14

EIRP Effective Radiated Isotropic Power. 16, 17

ERP Effective Radiated Power. 16, 17, 48

ETSI European Telecommunications Standards Institute. 16–18

FHSS Frequency Hoping Spread Spectrum. 6

FSK Frequency Shift Keying. 5, 7, 27

GFSK Gaussian Frequency Shift Keying. 7, 9

GPRS General Packet Radio Service. 14

HMI Human Machine Interface. 1

I^{2}C Inter Integrated Circuit. 40

IC Integrated Circuit. 5, 6, 8, 39, 40, 57

IoT Internet of Things. 5, 8, 14

IP Internet Protocol. 11

IPv6 Internet Protocol Version 6. 5

ISM Industrial Scientifical Medical. 2, 8

LBT Listen Before Transmit. 17, 18

LoRa Long-Range modulation. 21

LoS Line of Sight. 7

LPWAN Low Power Wide Area Network. 2, 8, 9

LRWPAN Low Rate Wireless Personal Area Network. viii, x, 2, 6, 7, 15

LTE Long-term Evolution. 14

MAC Medium Access Control. 3, 9, 10, 13

MCU Micro Controller Unit. 42, 52–54

NB-IoT Narrowband-IoT. 2, 14, 15

NF Noise Figure. 26

O-QPSK Orthogonal Quadrature Phase Shift Keying. 5, 7

OCV Open Circuit Voltage. 39, 40

P2P Point-to-Point. ii, 1, 30, 45

PA Power Amplifier. 29, 47, 48, 58

PHY Physical Layer. 3, 5, 9, 10, 13

POF Plastical Optical Fiber. 42

QoS Quality of Service. 10, 14

RF Radio Frequency. 21

RFTDMA Random Frequency and Time Division Multiple Access. 9

SF Spreading Factor. 24, 25, 33

SIG Special Interest Group. 6

SNR Signal-to-Noise Ratio. x, 21–23, 25, 27

SoM System on Module. 29

TCP Transmission Control Protocol. 11

TCXO Thermal Controlled Crystal Oscillator. 9, 23, 33, 49

UNB Ultra Narrow Band. 9

USB Universal Serial Bus. 40

WAN Wide Area Network. 8

Chapter 1

Introduction

This thesis work takes part in a project of energy an power monitoring in a domestic and small business environment; the system is composed by three different elements: the sensor, placed in proximity of the energy meter installed by the energy suppliers, the gateway, which is the centre of the system that collects all the information sent by the meter and an HMI. The information sent by the sensor shall be real-time. However, the focus of this work will be on the sensor node.

All the system is characterized by an easy-play installation, and for this reason the system and, in particular the meter, after the installation doesn't require any configuration by the final customer. To avoid any intervention from the user, the sensor is battery powered which should last at least 3 years without replacement or charging; this sensor will be integrated in a more extended network with other different type of sensors that will be developed in the future.

The thesis objective is studying, modeling and optimizing the point-to-point link between the meter and the gateway and maximizing the sensor battery life.

To achieve this goal a study of different technologies, standards and available protocols has been carried out. In the first part of the thesis different LPWAN and RF technologies will be introduced as possible solutions for the Point-to-Point (P2P) communication.

In the second part the LoRA technology will be analyzed in detail: a proprietary technology engineered by *Semtech*, characterized by a very high sensibility and low power performances.

In conclusion, the transmission model will be explained. Its core is a strategy responsible for planning the transmition of each message as function of energy/power variation measured on the meter, battery discharge estimation and compliance with band ETSI regulations.

Chapter 2

State of the art

2.1 Networks types overview

Initially, was conducted a study on the different network topology, technologies and standards.

Historically, LRWPAN is the oldest classification which includes a number of network solutions available for more than ten years and still present in the market. Low Power Wide Area Network (LPWAN) followed for the need to allow long range communications and finally Cellular IoT technologies (Narrowband-IoT (NB-IoT), LTE CAT-M) are growing up for the interest of mobile network operators in this business.

A possible classification of these networks could be based on the frequency band they use: free or proprietary. The former class is denominated Industrial Scientifical Medical (ISM) frequencies that could be used by everyone with some constrains such as a limited transmission power, duty cycle and bandwidth occupation; the latter class includes frequencies that are licensed and can be used only by the cellular network providers.

2.2 Network based on ISM frequencies

2.2.1 LRWPAN

The IEEE 802.15.4 standard is the base of many networks of this category: ZigBee, Thread and Bluetooth Low Energy (BLE). The standard cover the first two layers of the ISO/OSI stack, physical and data-link, and the upper layers are different for every protocol. Z-Wave is another network of this category that not comply with IEEE 802.15.4, but implement a proprietary stack, despite with similarities to other system.

These technologies are typically characterized by a mesh network topology (excluded BLE in its standard configuration), low rate and a low power. The mesh network topology could provide a more robustness on the paper, due to the presence of multiple path that link two nodes. A drawback is an higher computational power, required for forwarding and routing the messages, and some node need to be always awake in order to maintain the network stability [1].

Moreover, the data-rate has to be relatively high in order to overcome the delay caused by the forwarding process.

since a node failure doesn't affect the network stability, but a real redundant coverage can be obtained only with an accurate deployment of the network;

In any case the radio performance of these solutions are not adequate for our purpose since the product will be placed in a deep-indoor environment that may cause difficulty also to the first hop. And in addition to this, a mesh network is not applicable since to deploy this type of network is required a radio planning to place in the correct way the different nodes in order to reach a real redundant coverage. In fact device placement planning can not be done a priori in a network where nodes are distributed in unpredictable way and not controlled by a plan.

ZigBee

ZigBee is a protocol built on the top of the standard for short-range communications devices, IEEE 802.15.4 [2]. ZigBee specifications covers the upper layers of the protocol stack, while 802.15.4 describe the Medium Access Control (MAC) and Physical Layer (PHY) layers. Both 2.4 GHz and 868 MHz band could be used to implement the ZigBee protocol.

This protocol is thought to be used in application where low-throughput, low-power are required; although it is often advertised as a low-cost solution, this is not completely true due to the use of Direct Sequence Spread Spectrum (DSSS) modulation, described in detail in Chapter 3, that requires a stable clock source, usually expensive.

The main characteristic of ZigBee protocol is the support to the mesh network.

Figure 2.1 shows the protocol stack. This is composed by four layer and the PHY and MAC are covered by the IEEE 802.15.4 standard and the network and application layer are covered by ZigBee specifications document [3].

ZigBee could be configured in three different network topology: star, tree and mesh.

Three types of devices can be used in a ZigBee network:

- Coordinator: is the device with the greatest computational power and is unique in every network. This is the centre of the network and its task is to create and manage it and collect all the data incoming from the edge nodes;

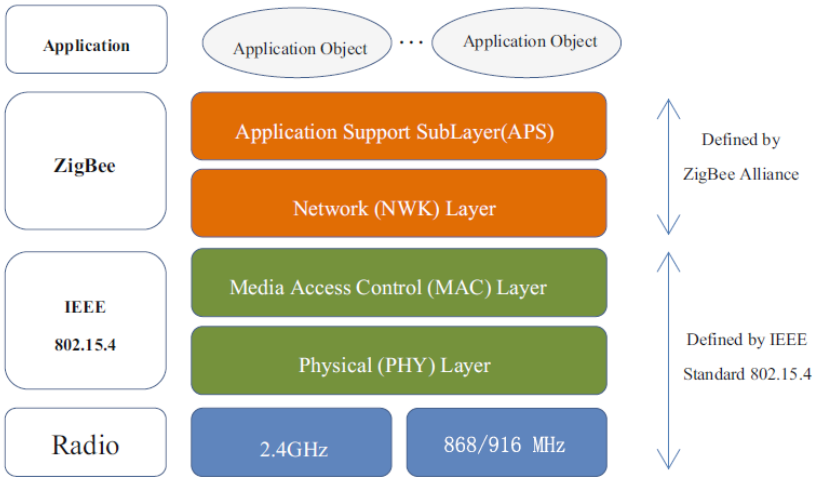

Figure 2.1. ZigBee protocol stack.

- Router: require less power than coordinator; it's able only to join an existing network but it can have children nodes and can manage their messages and redirect it to the coordinator;
- End node: are the simplest devices, in order to save energy they enter in a sleep mode if there aren't pending tasks.

In Figure 2.2 the different network topology and devices type are reported.

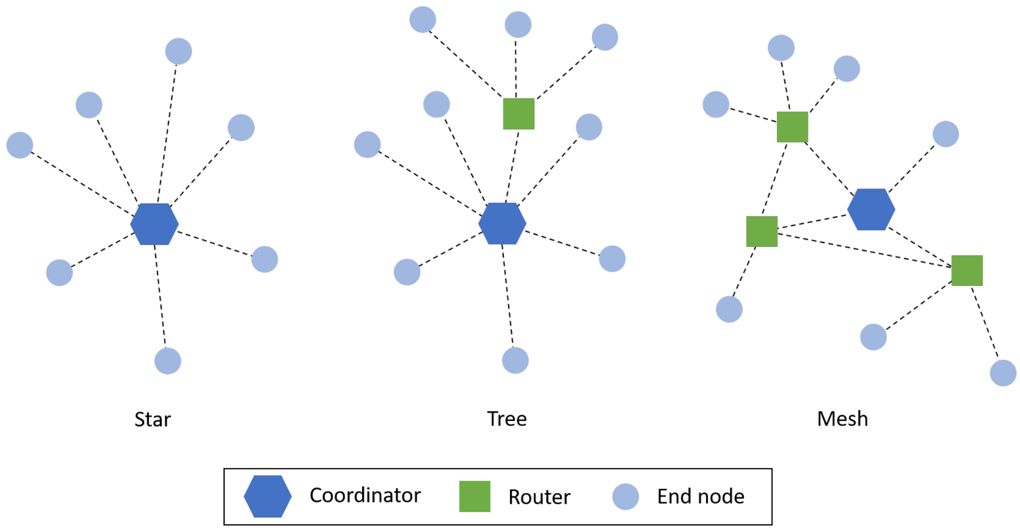

Figure 2.2. ZigBee configuration and devices types.

The main issue of the ZigBee is the use of a wide-band spectrum, due to the DSSS modulation, of 2 MHz [4]; the bandwidth occupation represents a major problem when the 868 MHz solution is chosen; instead, there isn't any problem when is being used the 2.4 GHz one because this band is wider than the 868 MHz one and allows 26 channels.

The problem of the 868 MHz band is that the ETSI regulations imposes the use of only one channel with the consequence of an high rate of collisions; moreover, to allow such wide bandwidth the power must kept low to be compliant.

Z-wave

Z-Wave is a proprietary Internet of Things (IoT) technology developed by *Sigma Designs* more that ten years ago. The Integrated Circuit (IC) that implements this protocol are supplied by *Sigma Designs* itself [5]. If on the one hand this bind developers and designer to a specific supplier, on the other it grants the interoperability of different devices based on Z-wave. Also the wireless standard is proprietary.

Z-wave uses a mesh network topology and the exploited frequency band in European region is the 868 MHz, one with a Frequency Shift Keying (FSK) modulation. The maximum data-rate is 9.6 kbps and the maximum range is 30 m per hop. Considering that the number of allowed hops are 4, the range in the best condition is 120 m .

Thread

Thread is a protocol developed by *Thread Group* and founded by seven companies: ARM, BigAss Fans, Freescale, Samsung, Yale, Silabs and Nest [5]. Thread is an open standard and specification details are available for free on the Thread Group website [6].

Thread, such as ZigBee, is implemented over IEEE 802.15.4 specifications, and is based on Internet Protocol Version 6 (IPv6) and 6LoWPAN. The network topology adopted is mesh and in a network more than one router/gateway could coexists avoiding that a node failure can compromise the communication [7].

The PHY layer is implemented with a Orthogonal Quadrature Phase Shift Keying (O-QPSK) modulation on a frequency of 2.4 GHz, the maximum reachable data rate is about 250 kbps. The range of a single hop is about 30 m and the maximum number of hops are 36. The upper limit of nodes in a network is more than 250.

Thread, as already said, is based on IPv6, to achieve a better energy efficiency the IPv6 is compressed with 6LoWPAN.

It can be seen that ZigBee and Thread have many common features. For this reason, with an adequate software adaptation, it's possible to implement a ZigBee network over Thread.

Figure 2.3 shows the different stack implementation.

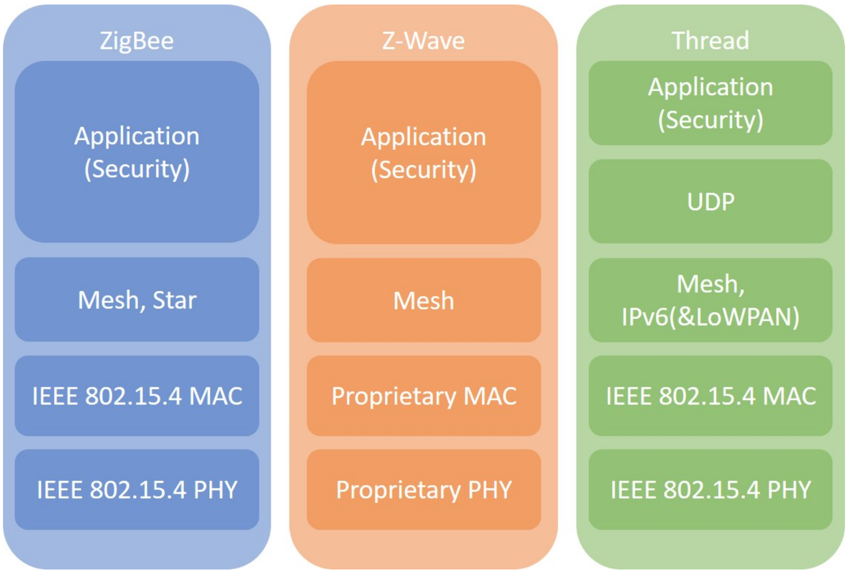

Figure 2.3. LRWPANs stacks.

Bluetooth Low Energy (BLE)

BLE is the Bluetooth Special Interest Group (SIG) response to the ever growing market's, and comes as a subset of Core Version 4.0 request of wireless connected, portable, energy efficient and low-cost devices. BLE comes as a subset of the Bluetooth (BT) Core Version 4.0 released in 2010 [8].

BLE reduces the classic BT peak, average and idle current.

Key features of BLE are:

- Interoperability: the BLE used frequency is 2.4 GHz, this ensure the possibility to use this technology in world wide applications. Moreover, SIG Core Version includes a strong procedure of interoperability testing process.

- Robustness: with classic BT, BLE has in common the use of Frequency Hoping Spread Spectrum (FHSS) to give a more robustness and avoid the interference with other devices that operates in the same bands, such as Wi-Fi.

- Low-cost: due to the small size of the IC is possible to design a module on a very small PCB with few external passive components.

- Bit rate: BLE is optimized to transmit short messages. Supports payloads from 8bytes to 27 bytes transferred at 1 Mbps. Useful when the real bit rate is low, in the order of 100 bps.
- Range: BLE offer a better range than classic BT. Theoretically could reach 60 m but in an effective implementation 30 m could be a realistic expectation.

The modulation scheme used by BLE is Gaussian Frequency Shift Keying (GFSK) in 2.4 GHz band. Respect to classic BT, BLE uses a modulation index of 0.5, that gives a better sensibility and lower power consumption.

To reduce the costs of BLE, the implemented channels are 40 instead of 79, and the bandwidth is 2 MHz instead of 1 MHz.

Table 2.2 is reported a comparison of different LRWPANs.

	ZigBee	**Z-Wave**	**Thread**	**BLE**
Frequency	2.4 GHz/868 MHz	868 MHz	2.4 GHz	2.4 GHz
Cod. sch.	DSSS	-	-	-
Modulation	O-QPSK(2.4 GHz) BPSK(868 MHz)	FSK	O-QPSK	GFSK
Output Pwr	20 dBm	5 dBm	20 dBm	10 dBm
Bandwidth	2 MHz	400 kHz/300 kHz	-	2 MHz
Range	30 m (indoor) 100 m (Line of Sight (LoS))	30 m/hop	30 m/hop	30 m (indoor) 60 m (LoS)

Table 2.1. LRWPANs comparison.

2.2.2 LPWAN

LPWAN is a type of network used to cover a large area and to connect low power node typically battery powered. This type of network is characterized by a low bit rate, low power consumption and extended range; these are the main differences with standard Wide Area Network (WAN) that are characterized by a moderate/high data-rate and an higher energy consumption.

Similar to the WAN, also with the LPWAN is possible to create a private network used to connect different end node sensors, but there are also third-parties services that can provide the infrastructure and network management, this latter solution allows a faster time-to-market because there is no need to design the gateway and manage the network.

Given the great expansion of IoT, a lot of different LPWAN has been developed, all with peculiar characteristics. Some of these are coordinated by alliances, while other are developed by private companies.

At the beginning, all the solutions was evaluated in order to make a comparison and choice the most suitable for the project.

The most popular LPWAN technology based on ISM frequencies that was in-depth examinated are

- Dash7
- Sigfox
- LoRAWAN

LoRaWAN is based on a LoRa physical layer instead Sigfox is based on a non-proprietary narrow band modulation, and DASH7 that doesn't require any particular modulation and is obtainable with common RF IC.

Dash7

DASH7 is a wireless protocol developed by DASH7 Alliance, the protocol is open and documentation and specification are freely available on the DASH7 website[9].

The frequencies used by DASH7 are the sub-GHz ISM ones, and for the Europe are the 433 MHz and the 868 MHz. DASH7 protocol was initially developed to be compliant to the ISO/IEC 18000-7 (Hence the name dash(-)7) and used in military logistic; at the current release the standard is no more compliant with the original standard.

DASH7 could work with different frequencies but the most often used is the 433 MHz. This frequency has a good concrete and metal penetration capability, although is required a bigger antenna.

The modulation used by DASH7 is the GFSK, there are 8 normal rate non-overlapping channels that can provide a data-rate of 55 kbps and 7 hi-rate channel (only 4 non-overlapping) that can provide a data-rate of 200 kbps.

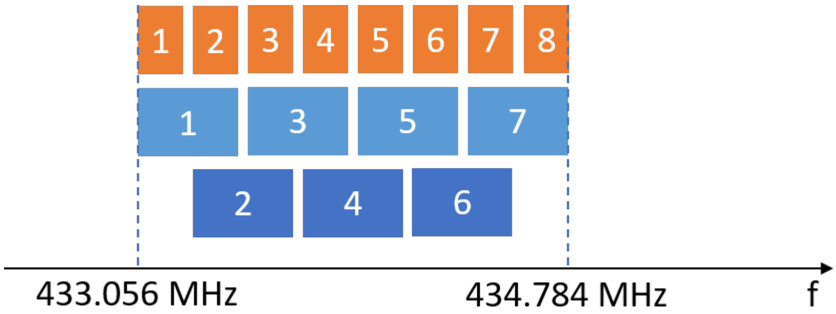

Figure 2.4. DASH7 channel allocation.

Sigfox

Sigfox is a LPWAN that employs as PHY the Ultra Narrow Band (UNB). With this technology the transmissions are performed using a Binary Phase Shift Keying (BPSK) modulation, with a low rate of 100 bps and the resulting transmitted signal bandwidth is 100 Hz.

The Sigfox occupied bandwidth is wider than the signal one; in fact, at every transmission the frequency carrier changes in a wide interval of 192 kHz. This characteristic gives Sigfox a more reliability and diversity to allow a better scalability of the network.

With UNB refers to a modulation where the frequency reference uncertainty is comparable with the signal bandwidth, this highlight the importance of a reliable and constant clock source. Typically, a Thermal Controlled Crystal Oscillator (TCXO) is required, and this drives up the cost.

Figure 2.5 shows the spectral occupation of 210 Sigfox signals.

The MAC used by Sigfox is Random Frequency and Time Division Multiple Access (RFTDMA)[10], the channel access take place without any contention, for this reason Sigfox could be considered an ALOHA based protocol except for the ability to change randomly carrier frequency.

To guarantee the delivery of the message, this must be sent three times on three different frequencies and the acknowledge of the message is sent on the same frequency by the base station to avoid too complex synchronization processes.

The Sigfox message shall consist of the following field

- Preamble, 4 bytes

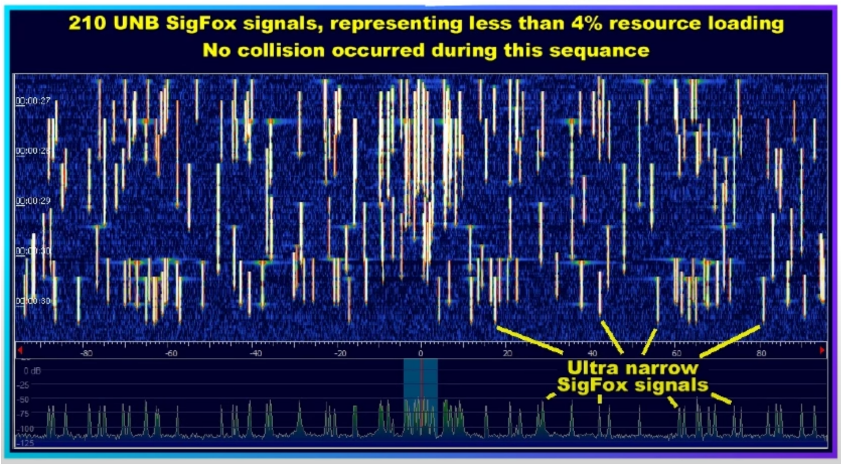

Figure 2.5. Sigfox messages.

- sync word, 2 bytes
- Sigfox ID, 4 bytes
- payload, 1 byte → 12bytes
- Hash, variable dimension
- CRC, 2 byte

Preamble	Sync w.	ID	Payload	Hash	CRC

Figure 2.6. Sigfox MAC layer frame.

It should be noted that the deployment of the Sigfox network is controlled by few operators (that often coincides with mobile network providers), and cannot be controlled in any way.

LoRaWAN

LoRaWAN represent the communication protocol, the MAC layer, and the architecture of the system. The LoRa represent the PHY and will be discussed in Chapter 3 [11].

The LoRaWAN could affect the battery lifetime, the security and the Quality of Service (QoS) of the network. The graphical representation of the protocol layers is reported in Figure 2.7

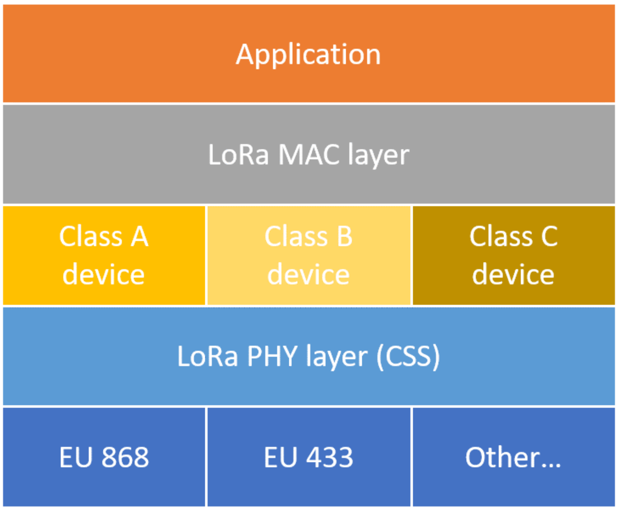

Figure 2.7. LoRa stack.

The typical network architecture is composed by different nodes connected to a gateway through LoRaWAN. The gateway instead is connected to a network server through a TCP/IP connection. As already explained the star architecture was adopted in order to waste less energy and increase battery life.

The message sent by the node is not directed to a specific gateway but, usually is received by more than one. All the required computations is moved towards the network server; then all the packets are forwarded by the gateway and the server will discard the duplicates and and performs the security check. Due to this implementation no handover is required.

In the LoRaWAN network the pure Aloha protocol is implemented to access the medium. With Aloha system the node could transmit whenever it has a data to transmit. Since that no control is done on the channel, collisions are inevitable. To inform the end node of the successful reception of the message an acknowledge is sent by the gateway[12] back to end node.

The Aloha method is asynchronous and avoid the need of node synchronization as occurs in cellular network. This prevent a frequent wake-up event and preserve more energy.

As will be explained in Chapter 3 the LoRa modulation is based on a spreading technique. The two variables are: the spreading factor and the bandwidth, most configurations are orthogonal, a graphical representation is reported in Figure 2.8 [13].

The orthogonality allows the coexistence of many nodes on the same channel but with different data-rate. It is required a gateway able to receive simultaneous messages with different data-rate and on different channels.

spreading factor (SF) and bandwidth (BW) in kHz

SF		07	08	09	10	11	12	07	08	09	10	11	12	07	08	09	10	11	12
	BW	125	125	125	125	125	125	250	250	250	250	250	250	500	500	500	500	500	500
07	125	x								x								x	
08	125		x								x								x
09	125			x								x							
10	125				x								x						
11	125					x													
12	125						x												
07	250							x								x			
08	250								x								x		
09	250	x								x								x	
10	250		x								x								x
11	250			x								x							
12	250				x								x						
07	500													x					
08	500														x				
09	500							x								x			
10	500								x								x		
11	500	x								x								x	
12	500		x								x								x

Figure 2.8. LoRa settings combinations orthogonality.

To increase this variability and decrease the collision probability, in LoRaWAN protocol, is implemented an adaptive data-rate. This allows the optimization the channel occupancy because the data rate can be increased and then the time on-air is reduced; this has a positive results also on the battery consumption.

LoRaWAN has three different classes of end-devices to address the various needs of applications:

- Bi-directional end-devices (Class A): End-devices of Class A allow for bidirectional communications and, for this reason, each end-device's uplink transmission is followed by two short downlink receive windows. The transmission slot scheduled by the end-device is based on its own communication needs with a small variation based on a random time basis (ALOHA-type of protocol). This Class A operation is the lowest power end-device system for applications that only require downlink communication from the server shortly after the end-device has sent an uplink transmission. Downlink communications from the server at any other time will have to wait until the next scheduled uplink.

- Bi-directional end-devices with scheduled receive slots (Class B): End-devices of Class B allow for more receive slots. In addition to the Class A random receive windows, Class B devices open extra receive windows at scheduled times. In order for the End-device to open its receive window at the scheduled time, it receives a time synchronized Beacon from the gateway.

- Bi-directional end-devices with maximal receive slots (Class C): End-devices of Class C have nearly continuously open receive windows, only closed when transmitting. Class C end-device will use more power to operate than Class A or Class B but they offer the lowest latency for server to end-device communication[14].

The graphical representation of different nodes is reported in Figure 2.9.

It should be noted that LoRaWAN does not enable device-to-device communications: packets can only be transmitted from an end-device to the network server, or vice-versa. Device-to-device communication, if required, must thus be sling-shot through the network server (and consequently, by way of two gateway transmissions) [15].

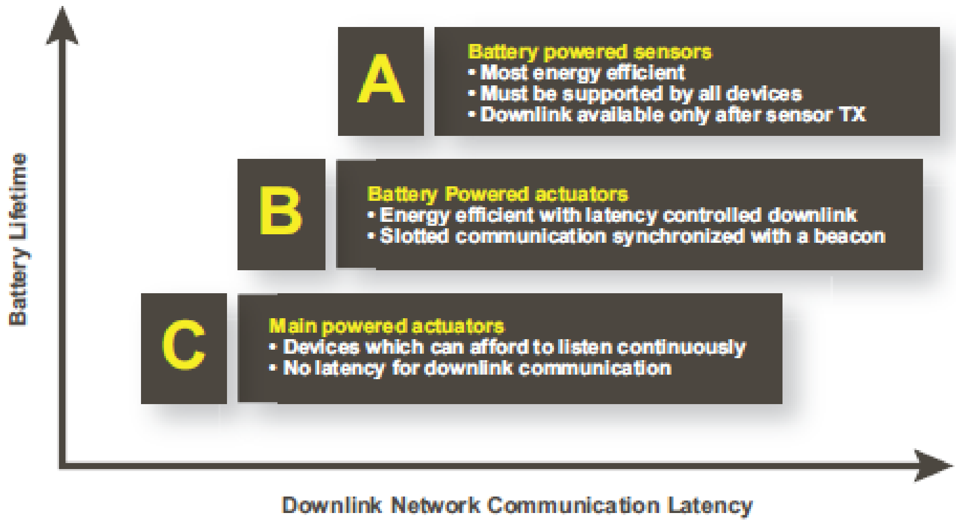

Figure 2.9. LoRa settings combinations orthogonality.

The most suitable operation mode for the application could be the Class A type, and then will be in-depth analyzed.

Class A message The MAC payload is embedded in a PHY layer frame, reported in Figure 2.10, that will be discussed in Chapter 3. The MAC payload is composed as in Figure 2.11.

The three main field of the MAC frame are:

Preamble	PHDR	PHDR CRC	PHY Payload	CRC

Figure 2.10. LoRa radio physical layer frame.

MHDR	MAC Payload	MIC

Figure 2.11. LoRa radio MAC layer frame.

- MAC Header (MHDR field, 3 bits), composed by 1 byte and describe the message type and the LoRaWAN specification version (Major field, 2 bits);
- MAC Payload that could be composed by 7 to N bytes;
- Message integrity code (MIC) of 4 bytes.

2.2.3 Network based on licensed frequencies

Aside from technology that exploit the ISM frequencies, there are also the cellular technology that works on licensed frequencies. This standard are described by the 3rd Generation Partnership Project (3GPP) organization. The two standard introduced for IoT are: EC-GSM ,Long-term Evolution (LTE) CAT-M and NB-IoT.

EC-GSM was designed in order to adapt the actual General Packet Radio Service (GPRS) and Enhanced Data rates for GSM Evolution (EDGE) systems to the necessities of IoT, such as a better coverage (better sensitivity) and lower power consumption, however the typical data-rate is high and is not suited for very low power devices.

Even if designed for IoT LTE CAT-M is intended to be used in case in which is required a sustained data-rate, although less than EC-GSM and quite low latency, also in this case a very low consumption is hardly achievable. Besides this, in Italy this type of network is emerging and the deployment is not already complete.

The NB-IoT will be analyzed in depth in the following part.

NB-IoT

The needs that led to the development of the NB-IoT are the improvement of the sensitivity respects to the other cellular technologies and a lower energy consumption.

In NB-IoT, therefore, there isn't the concept of QoS, in fact is not suited to applications where the low latency and the delivery of the packet must be assured.

The occupied bandwidth is 180 kHz, this correspond to one resource block of LTE, and the possible operation modes are:

- *in-band operation* when, NB-IoT block, stand within an LTE carrier;
- *guard-band operation* when exploit the guard band of LTE;
- *stand-alone* when is outside LTE carriers or inside GSM band.

This different configuration are reported in Figure 2.12.

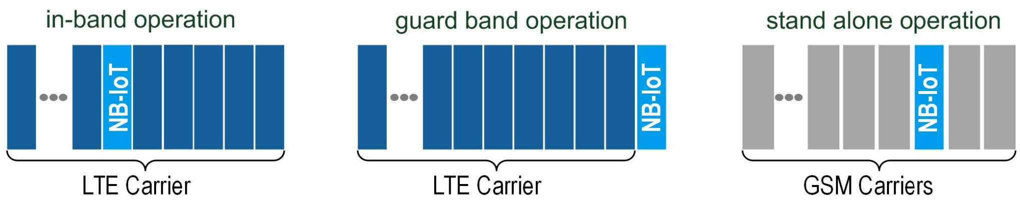

Figure 2.12. Different type of operations in NB-IoT.

With NB-IoT is not possible to use TCP/IP but the communication occurs only with UDP/IP sockets.
This technology solution was discarded due to the delays of the national network deployment and the excessive management costs.
Table 2.2 is reported a comparison of different LRWPANs.

	Dash7	**Sigfox**	**LoRaWAN**	**NB-IoT**
Frequency	433 MHz	868 MHz	868 MHz	same as LTE
Cod. sch.	-	UNB	CSS	-
Modulation	GFSK	BPSK	CSS	OFDM
Output Pwr	10 dBm	20 dBm	20 dBm	23 ± 3 dBm
Ch. bandwidth	200 kHz 400 kHz	100 kHz	125 kHz 250 kHz 500 kHz	180 kHz
Data-rate	50 kbps 200 kbps	120 bps	from 30 kbps 300 bps	20 kbps 250 kbps

Table 2.2. LRWPANs comparison.

2.3 Network analysis results

The previously discussed technology, although promising, are not adequate to our purpose.

Sigfox was discarded because the low number of message allowed per day, the necessity of a network provider and associates costs.

Dash7 and Symphony Link are thought to be more reliable and with more complex management of the network; this is not compatible with our system that require a fast response accepting a low reliability of the message delivery.

The more adapt could have been the LoRaWAN protocol, but the overhead of every message lead to longer transmission time and to a lower real bit-rate.

At the end a custom protocol was developed to optimize the transmission and to best fit the network to the application. The used frequency is in the 868 MHz-870 MHz band; these frequencies was chosen in order to have a good concrete and wall penetration but maintaining a good amplification and antenna efficiency.

2.4 RF technology and radio regulations

As already said the frequency band used for the link between the Reader and the meter is the 868 MHz - 870 MHz one.

This imply that the system have to comply with the regulations; in particular with the European ones since that the final product will not sold outside of this region.

The European regulatory agencies are the European Telecommunications Standards Institute (ETSI), the European Commission (EC) and Electronic Communications Committee (CEPT/ECC).

In particular the ETSI and CEPT/ECC, give constrains in term of Effective Radiated Power (ERP) power and of duty cycle for every sub-bands, here indicated as g, $g1$, $g2$, $g3$, $g4$.

The limits are reported in Figure 2.13.

2.4.1 Power limitations

The emissions of a device could be estimated in three different ways:

- Could be evaluated the electrical field strength, indicated with the letter E and expressed in dBμV/m, at specific distance from the Device Under Test (DUT);

- using the Effective Radiated Isotropic Power (EIRP), this represent the required power that should be provided to an isotropic antenna to generate

Band	Edge Frequencies		Field Power	Spectrum Access	Band Width
g (Note1,2)	863 MHz	870 MHz	+14 dBm	0.1% or LBT+AFA	7 MHz
g (Note2)	863 MHz	870 MHz	-4.5 dBm / 100 kHz	0.1% or LBT+AFA	7 MHz
g (Note2)	865 MHz	870 MHz	-0.8 dBm / 100 kHz	0.1% or LBT+AFA	5 MHz
	865 MHz	868 MHz	+6.2 dBm / 100 kHz	1% or LBT+AFA	3 MHz
g1	868.0 MHz	868.6 MHz	+14 dBm	1% or LBT+AFA	600 kHz
g2	868.7 MHz	869.2 MHz	+14 dBm	0.1% or LBT+AFA	500 kHz
g3	869.4 MHz	869.65 MHz	+27 dBm	10% or LBT+AFA	250 kHz
g4	869.7 MHz	870 MHz	+14 dBm	1% or LBT+AFA	300 kHz
g4	869.7 MHz	870 MHz	+7 dBm	No requirement	300 kHz
Note1: Modulation bandwidth ≤ 300 kHz is allowed. Preferred channel spacing is ≤ 100 kHz. Note2: Sub-bands for alarms are excluded (see ERC/REC 70-03 Annex 7).					

Figure 2.13. ETSI regulations.

the same electric field as measured one, generated by the DUT. The EIRP is computed as follow

$$EIRP\,[\text{dBm}] = P_t - L + G$$

where P_t is the transceiver output power, L represents the loss on the cable and mismatch and G is the gain of the antenna, all the variable are expressed in dB;

- using ERP, the ERP is computed as EIRP but using an half-wave dipole instead of an isotropic radiator. Since that the half-wave dipole has a gain of dBi (respect an isotropic radiator), the ERP cold be calculated as follow

$$ERP\,[\text{dBm}] = EIRP - 2.15\,\text{dBm}$$

ETSI regulation adopts the last method, the ERP.

2.4.2 Time limitations

The duty cycle limit represents the time, expressed as a percentage value, that a device can transmit during a period of one hour; for example if the DC is 1% the device is authorized to transmit 36 seconds.

In particular, the frequencies used by the device are the $g1$ and $g2$, the transmission time limits for these are reported in Table 2.3.

This limit could be overridden by an implementation of LBT+AFA strategy.

With Listen Before Transmit (LBT), the device, before the transmission, must control if the channel is busy; this can be done measuring the RSSI. This procedure is easily implementable, but the problem is inherent to the spread spectrum

sub-band	DC	t_{TX}
g1	1 %	36″
g3	10 %	360″

Table 2.3. Allowed transmission time over 1 hour.

modulation, in this case a signal could be reconstructed also if below the noise floor of the receiver; then a weak signal may not be detected. A partial solution could be use the Channel Activity Detection (CAD) functionality, detailed in the next chapter.

Instead, Adaptive Frequency Agility (AFA) is the capacity of the device to switch the channel to avoid crowded ones; the implementation of this could be less trivial because could lead to a misalignment of transmitter and receiver.

In the final system was applied only a LBT strategy to avoid collision with other packets but not AFA, so the duty cycle limits have to be respected.

The ETSI regulation imposes also a limit on the occupied bandwidth. As already said, for our device the used sub-bands are the $g1$ and $g2$, as defined in Figure 2.13.

For these bands the limits are 600 kHz and 250 kHz.

2.4.3 ETSI limits applied to LoRa signal

The sub-band $g1$ allows defining three channels with a LoRa bandwidth of 125 kHz (Figure 2.14), one channel with a bandwidth of 250 kHz (Figure 2.15) and, with an appropriate setting of the spectral filter, one channel with 500 kHz (Figure 2.16).

For the sub-band $g3$ only one channel is allowed with a bandwidth of 125 kHz, in Figure 2.17 is shown the certification report of the module *SX1272*[16] that has the same RF front-end of the *SX1276*.

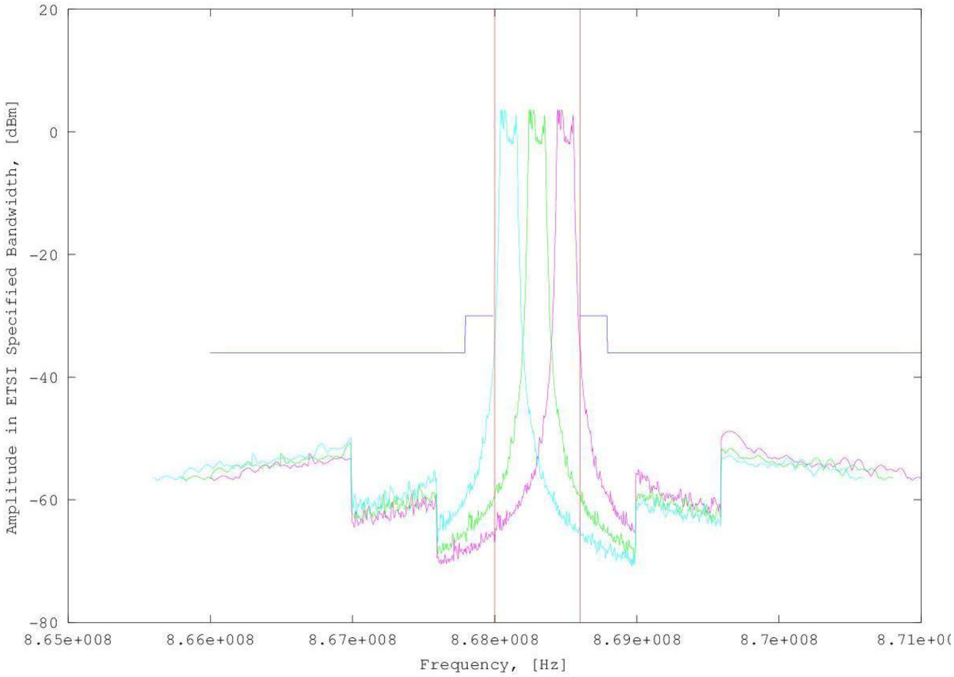

Figure 2.14. Sub-Band $g1$ 13 dBm RF Output Power 125 kHz Bandwidth.

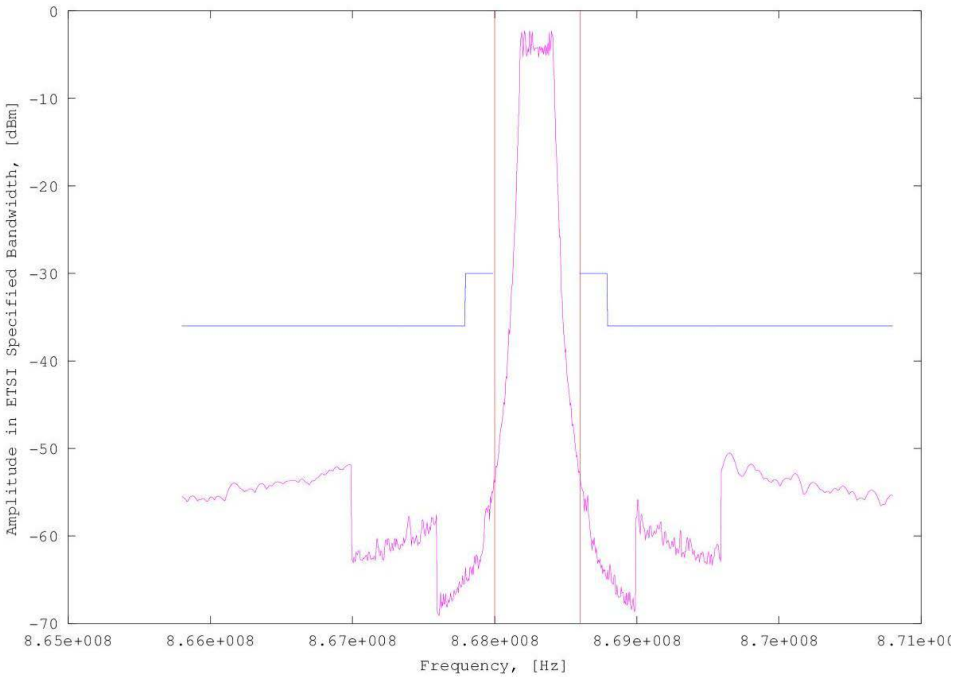

Figure 2.15. Sub-Band $g1$ 13 dBm RF Output Power 250 kHz Bandwidth.

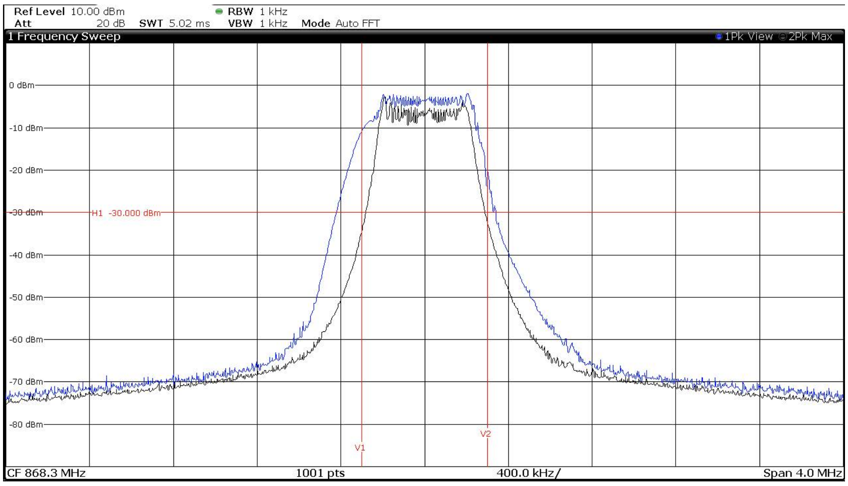

Figure 2.16. Sub-Band $g1$ 13 dBm RF Output Power 500 kHz Bandwidth with spectral filtering active.

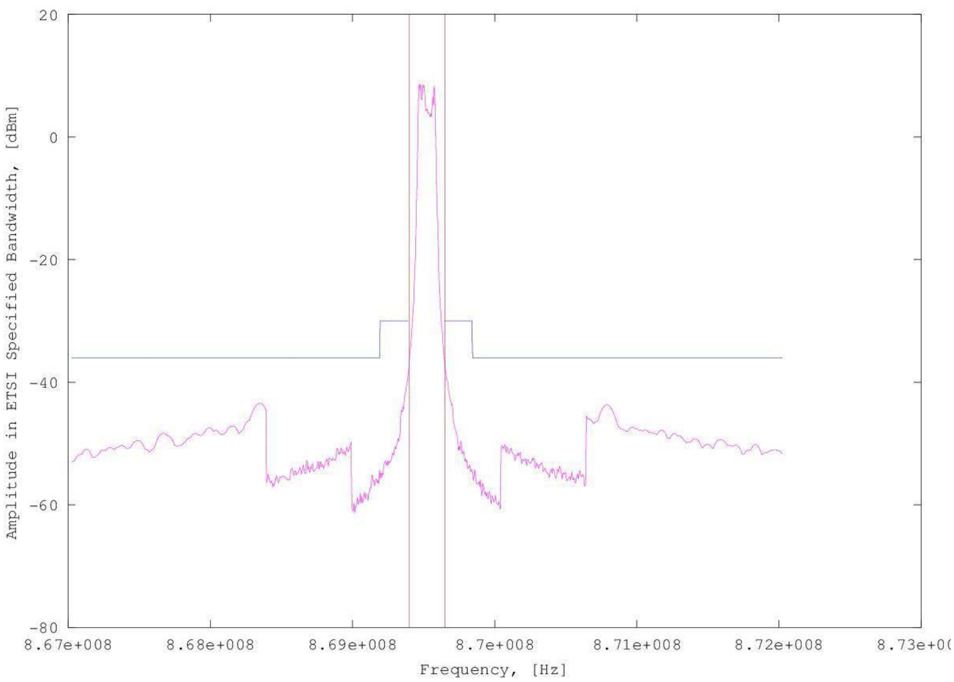

Figure 2.17. ETSI regulations.

Chapter 3

LoRa technology

3.1 Overview

Long-Range modulation (LoRa) is a modulation technique, designed by Semtech, that exploits a spread spectrum scheme that derives from DSSS, historically used in the radar technologies, in which data rate and sensitivity are inversely proportional, fixed the bandwidth.

With this modulation it is possible to obtain a variable data-rate changing the spreading factor and this lead to a trade off between range, power and bit-rate, therefore, allowing an optimization of network performance based on the environment within a fixed bandwidth.

LoRa represent the physical layer only, so it doesn't concern the protocol implemented in the higher layer. This is a flexibility that allow to use LoRa as physical layer for different network system.[17]

In fact this technology was chosen to implement our custom protocol.

3.1.1 Spread Spectrum theory

Increasing the bandwidth it is possible to compensate the degradation of SNR of a Radio Frequency (RF) link; the basis of this statement could be found in the Shannon Hartley theorem.

Shannon Hartley theorem

Starting from the assumption that thermal noise is the main noise source, it is possible to consider the Additive White Gaussian Noise (AWGN) channel applicable to various scenarios. The capacity of this type of channel is given by Equation 3.1.

$$C = B \log 2 \left(1 + \frac{S}{N} \right) \tag{3.1}$$

where B is the bandwidth, S is the signal power and N is the noise power and then the $\frac{S}{N}$ the signal to noise ratio. The dimension of the result is $\frac{bit}{s}$ [18].

The Equation 3.1 could be manipulated to obtain Equation 3.2.

$$\frac{C}{B} = 1.433 \cdot \frac{S}{N} \tag{3.2}$$

From Equation 3.2 it can be seen that, fixing the SNR, to have a error free channel the bandwidth has to be increased.

The typical application of spread spectrum technique could be found in the DSSS, where the carrier phase of original signal is modulated by a code sequence, then the output signal is obtained multiply the data signal with a chip sequence that represent the spreading code. Chip signal is more fast than the original one, this lead to have an output with a bandwidth much larger than the original one.

A summary of the modulation process is represented in Figure 3.1

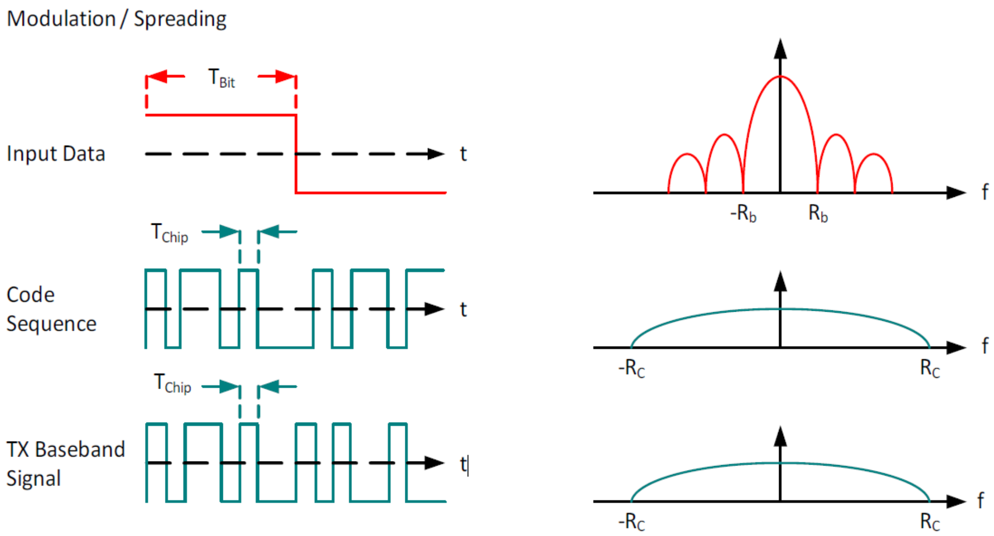

Figure 3.1. DSSS modulation process.

The process is reversed at the receiver, where the incoming signal is again multiplied with the local chip sequence to obtain the original signal. It's important that the receiver chip sequence is the same as that was used by the transmitter to extrapolate the information in the correct way. The reverse process is shown in Figure 3.2.

The width of spreaded bandwidth is characterized by the *chips per bit* ratio. A parameter, called processing gain, could be defined as the ratio between the chip rate (R_C), expressed as chips/sec, and the desired bit rate (R_b), expressed as

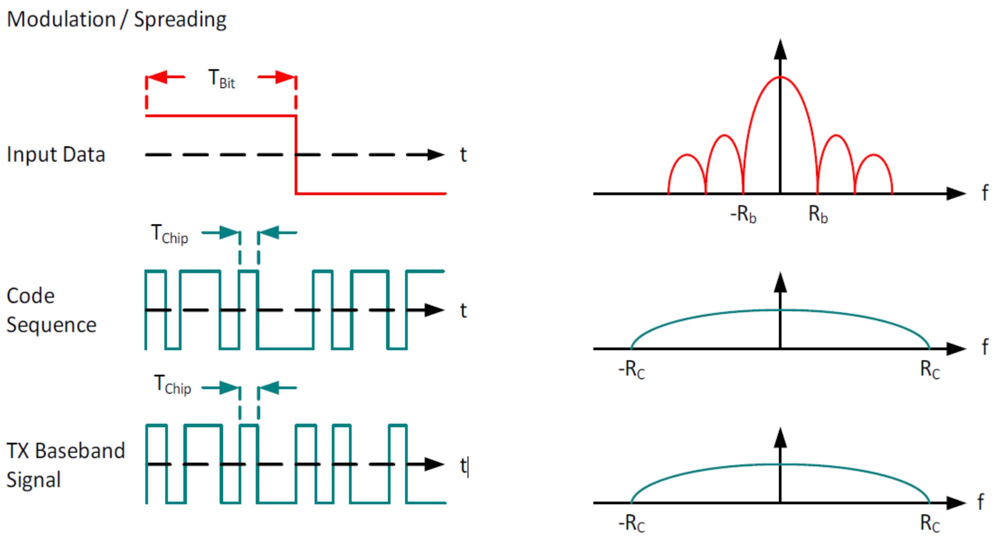

Figure 3.2. DSSS de-modulation process.

bit/sec.

$$G_p = 10 \log 10 \left(\frac{R_C}{R_b} \right) \tag{3.3}$$

The processing gain is expressed as dB.

The spreading process lead to two advantages. The former is the gain obtained for the transmission; in fact the receiver is able to reconstruct the signal also if the SNR is below zero. The latter is that narrowband interfering signals, during the de-modulation process is spread beyond the information bandwidth, then removed by adequate filtering process.

The main disadvantages of the DSSS modulation are: the necessity of an accurate clock source, such as a TCXO, that require more energy and the slow signal reconstruction process.

3.1.2 LoRa Chirp Spread Spectrum

The main idea behind the LoRa CSS modulation, differently from DSSS, where the spreading sequence was digital, is that the signal is multiplied by a linearly varying tone through time. This lead to a signal with larger bandwidth than the original.

This spreading of the symbol over a wider bandwidth give a more robustness towards narrowband noise and interferers.

The duration of the frequency sweep is characterized by a parameter called Spreading Factor (SF) and Bandwidth (BW).

The symbol time is determined by the spreading factor: if this is increased by one the symbol time duplicates. Instead it is inversely proportional to the bandwidth, because increasing it increases the rate of the chirps and therefore the bitrate. This lead to a trade off between transmission time, bandwidth and spreading factor.

On the one hand, increasing the symbols time the message leads to a more reliable link thanks to a higher robustness, but on the other hand, a longer symbol means a more delicate synchronism between transmitter and receiver that could lead to symbol errors.

SF could be seen as the number LoRa's symbols used to transmit a bit of information.

The symbol time could be expressed as in 3.4.

$$t_{sym} = \frac{2^{SF}}{BW} \tag{3.4}$$

As already said the preamble has an offset of 4.25 symbols, as reported in Equation 3.5 where $N_{preamble}$ is the user defined preamble. The duration of the preamble is a critical parameter because the higher it is, the higher the probability is for the receiver to detect an incoming message.

$$t_{preamble} = (N_{preamble} + 4.25) \cdot t_{sym} \tag{3.5}$$

The number of symbols of the LoRa frame could be computed in a more complicated way, since it depends on many variable, as shown in Equation 3.6.

$$N_{payload} = 8 + max\left(\left\lceil \frac{8PL - 4SF + 28 + 16CRC - 20H}{4 \cdot (SF - 2DE)} \right\rceil \cdot (CR + 4), 0\right) \tag{3.6}$$

In Equation 3.5 the variables are:

- PL is the number of payload bytes;
- SF is the spreading factor, this can vary from 6 to 12;
- CRC is a binary value that indicates if the Cyclic Redundancy Check (CRC) is enabled or not, if it's 0 the CRC is enabled, if it's 1 the CRC is disabled;
- H is a binary value that indicates if the explicit header is enabled, the header is used to carry the information about the packet, when it's 0 the header is enabled, when it's 1 is disabled;

- DE is a binary value that indicates is low data rate optimization is active or not, this is required when very long symbols is sents (e.g.: SF=12, BW=125) to guarantee a correct synchronization beetween transmitter and receiver;
- CR represent the coding rate (1: 4/5 4: 4/8).

Therefore, the payload transmission last for the number of symbols of the payload multiplied by the symbol time as in Equation 3.7.

$$t_{payload} = N_{payload} \cdot t_{symbols} \tag{3.7}$$

At the end, the total transmission time is the sum of preamble and payload transmission time.

$$t_{TX} = t_{preamble} + t_{payload} \tag{3.8}$$

LoRa bit rate performance

The LoRa modulation bit rate, considering the Equation 3.4 could be evaluated as expressed by Eq. 3.9

$$DR = SF \cdot t_{sym} \cdot CD \tag{3.9}$$

Where Coding Rate (CR) is computed as

$$CR = \frac{4}{cr + 4}$$

with *cr* the user imposed coding rate that varies from 1 to 4. In table 3.1 are reported different bit rate for different configurations, fixed the preamble, coding rate and payload dimension.

The transmission time of 13 bytes payload with a 8 (+4.25) symbols of preamble is reported in Figure 3.3.

LoRa sensitivity performance

As previously said, the nature of LoRa allows the reconstruction of a signal also if this is below the noise floor. The minimum SNR is influenced by the choice of the SF. This relation is reported in Table 3.2.

The choice of SF influences the receiver sensitivity that is computed as in Equation 3.10 .

$$S = -174 + 10 \log 10(BW) + NF + SNR \text{ [dBm]} \tag{3.10}$$

Spreading Factor	125 kHz	250 kHz	500 kHz
7	5.5 kbps	11 kbps	22 kbps
8	3.1 kbps	6.3 kbps	12.5 kbps
9	1.8 kbps	3.5 kbps	7 kbps
10	1 kbps	2 kbps	2 kbps
11	530 bps	1 kbps	2 kbps
12	300 bps	600 bps	1.2 bps

Table 3.1. LoRa bit rates with fixed preamble (8), CR (4/5) and payload (13 bytes)

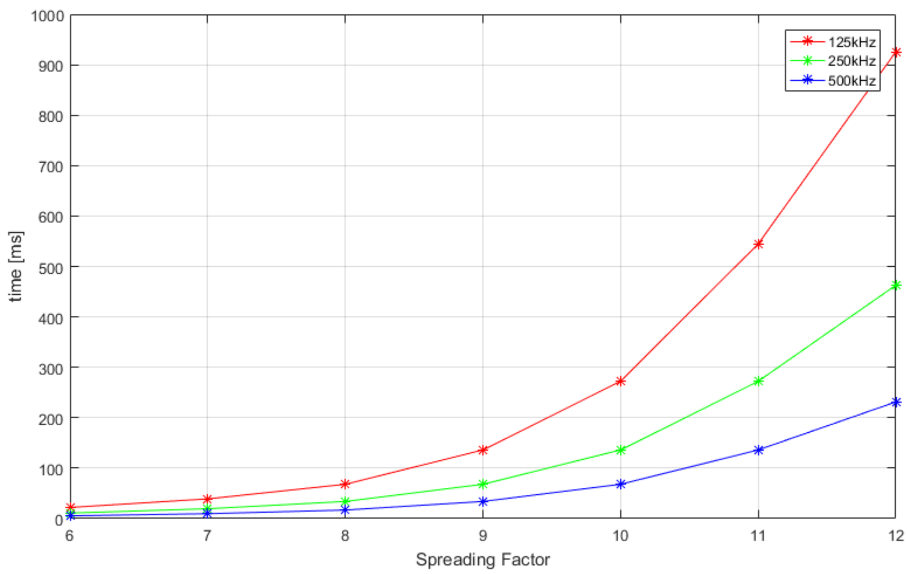

Figure 3.3. Tranmission time.

where the first term, -174 is the absolute noise floor at 1 Hz, and is computed as reported in Equation 3.11

$$NF_{absolute} = 10 \cdot \log 10(1000 \cdot k \cdot T \cdot BW) \ \text{[dBm]} \tag{3.11}$$

where k is the Boltzman's constant ($\approx 1.38 \cdot 10^{-23}$), T is the room temperature (293 K) and BW the bandwidth.

Instead, the Noise Figure (NF) term that appears in Eq. 3.10 is the noise

SF	SNR
7	−7.5 dBm
8	−10 dBm
9	−12.5 dBm
10	−15 dBm
11	−17.5 dBm
12	−20 dBm

Table 3.2. Correlation between spreading factor and SNR.

figure of the receiver that is a variable parameter with a typical value of 6 dBm. In Figure 3.4 could be seen the comparison between LoRa modulation and a FSK one.

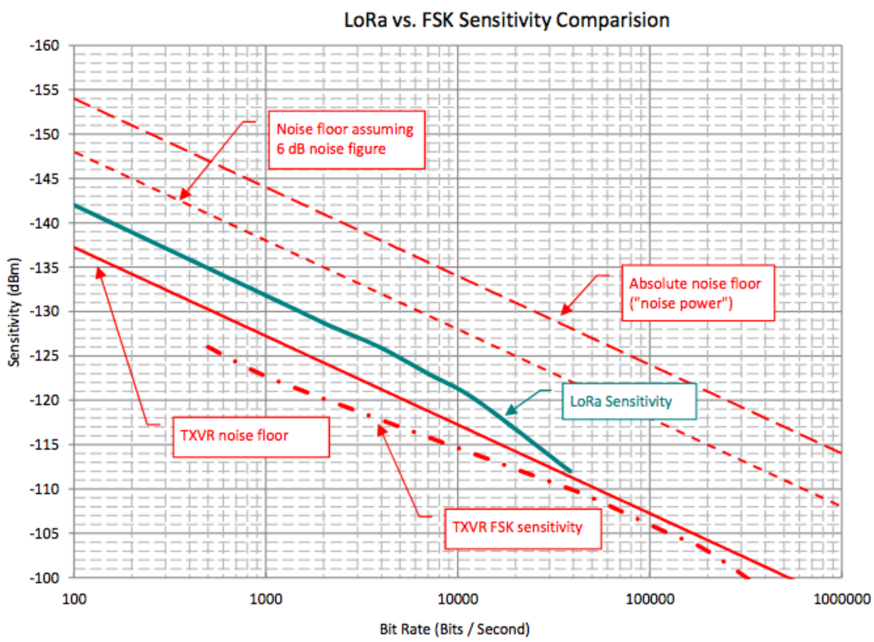

Figure 3.4. LoRa and FSK comparison.

3.2 LoRa Modem

The LoRa modem implements two types of packet: the explicit and the implicit types.

- The explicit type contains a short header in which some information of the packet itself are reported, such as the number of bytes of the payload, the forward error correction coding rate and the presence of the optional 16-bit CRC of the paylod; the exploiting of the explicit header is needed in case of a non-fixed message; moreover, the header contains also its own CRC in order to identify invalid headers;

- the implicit type has not the header, but the receiver has to know a priori the characteristic of incoming message.

The LoRa frame format is shown in Figure 3.5.

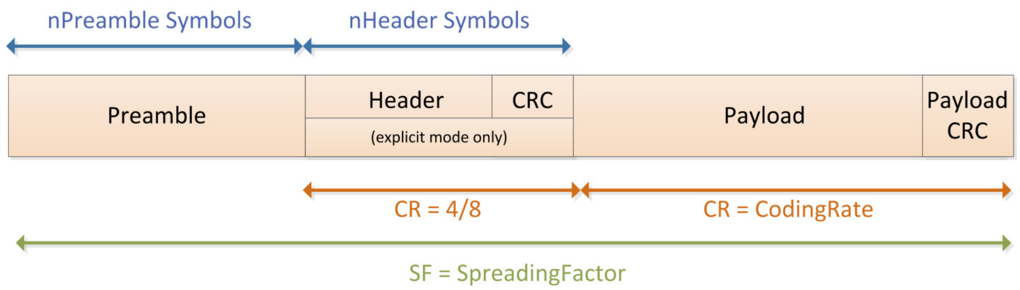

Figure 3.5. LoRa frame.

The first field is the preamble, that is used to synchronize the receiver with the incoming message. The typical value is 12 symbols and it is important to notice that there is a fixed offset of about 4 symbols to the set preamble (eg.: if set preamble is 6 the actual one is about 10). This field could assumes values from 10 to 65535 (2^{16})

The second field is the header which contains information about the following payload.

The packet payload is a variable-length field that contains the actual data coded at the error rate as specified in the header in explicit mode or as selected by the user in implicit mode. An optional CRC may be appended[19], in order to check out the correctness of the incoming message.

3.3 Main Semtech chips

LoRa is a proprietary and patent technology, this imply that the IC that can use this modulation are few and produced only by Semtech itself.

The most popular is the SX127x family, that comprehends *SX1276* and *SX1272* that are the most suitable for the project.

With this chip, it can be obtained a sensitivity below −148 dBm in certain conditions and settings. In real applications a sensitivity of −136 dBm could be achieved. In the module a Power Amplifier (PA) is integrated, able to provide an output of 20 dBm.

These factors can guarantee a considerable link budget and then provide a stable link also in deep-indoor application.

The used chip for the project is the SX1276, embedded in the System on Module (SoM) CMWX1ZZABZ produced by Murata. The schematic of the module is shown in Figure 3.6.

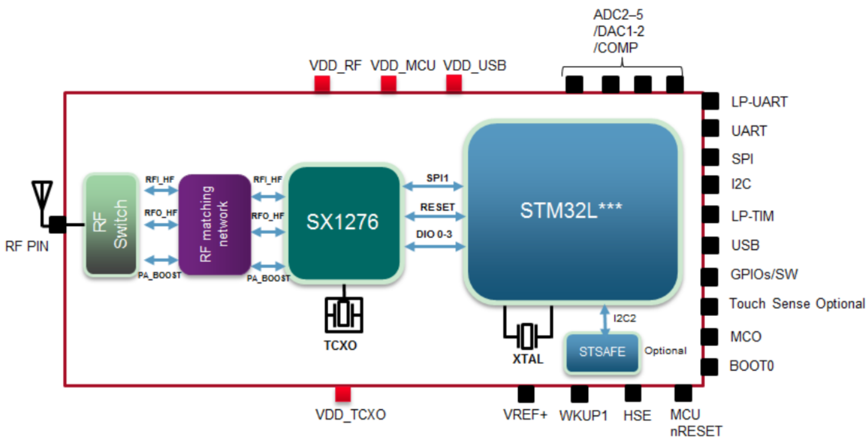

Figure 3.6. Murata module schematic.

A SoM was chosen in order to have a faster time to market of the product. The module includes a Low Power MCU STM32L082CZ produced by ST Microelectronics, the Semtech's SX1276 with relative matching network and RF switch to select RX/TX path.

The transceiver, $SX1276$, has a sensitivity that is reported in Figure 3.7.

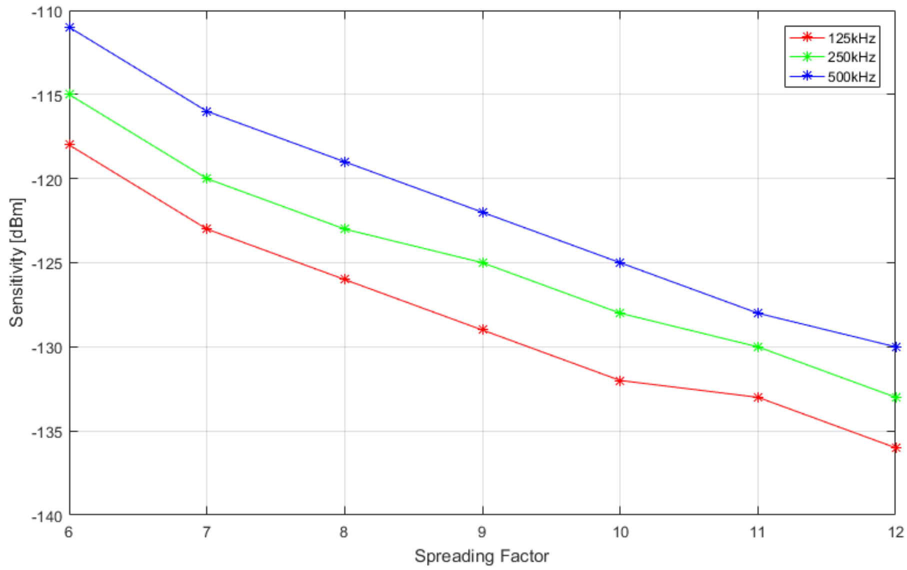

Figure 3.7. Transceiver sensitivity.

3.3.1 LoRa P2P tests

To validate the choice of LoRa technology some tests have been conducted in plausible environments. The first test site is a ten floors building, whose picture is reported in Figure 3.8.

The test setup is: transmitter and receiver with a lambda/4 antenna, the former with horizontally positioned antenna and the latter with vertical orientation; the transmitter was positioned at the floor 0 and the receiver at floor 10. The results of the tests are reported in Table 3.3.

The results seem good, but the building is narrow and for the signal, there is a clear path outside the building itself.

The second test has been conducted in the EMA building, the setup was similar as for first site. The transmitter was placed at level -1, in the building garage, and the receiver on the roof (+3). A picture of the test site is reported in Figure 3.9.

The test results are reported in Table 3.4. From these, it could be seen that, also with only three floor, this type of building could cause some troubles due to the strong presence of reinforced concrete and thick structures typical of the pre-assembled buildings.

Figure 3.8. 10 floors building test site.

Power [dBm]	SF	Tx pkts	Rx pkts	PER [%]
5	7	150	15	90
5	8	150	109	27.3
5	9	150	136	9.3
10	7	150	150	0
10	8	150	150	0
10	9	150	150	0

Table 3.3. Test result in ten floors building site.

Figure 3.9. EMA building test site.

Power [dBm]	SF	Tx pkts	Rx pkts	PER [%]
10	9	100	0	100
10	10	100	16	84
10	11	100	80	20
10	12	100	72	28
15	9	100	80	20
15	10	100	78	22
15	11	100	92	8
15	12	100	99	1
20	9	100	82	18
20	10	100	93	7
20	11	100	100	0
20	12	100	100	0

Table 3.4. Test result in EMA building site.

3.3.2 Measurements

Some measurements have been done in order to characterize the system, these are the starting point for the model computations. In particular some current, power and energy measurements have been conduced. A picture of measurement set-up is reported in Figure 3.10.

The instrument used to carry out the measures is the *CX3324*, this is a current waveform analyzer; is equipped with 16 bits ADCs, and a bandwidth of 200 MHz.

The device used to perform the tests is a evaluation board, designed by *STMicroelectronics*, B-L072Z-LRWAN1. This board has three jumpers on each trace that carry the current to the MCU, USB and RF. The measurement has been done, in particular, on the RF plus USB line. The USB was included because the pin that provide the supply voltage to the TCXO is a pin powered by VDD_{USB}; nothing more is connected to this net.

In Figure 3.11 is reported the current waveform acquisition for the worst, in term of transmission time, parameters, and therefore SF 12, bandwidth 125 kHz and output power at 20 dBm. Instead, in Figure 3.12 the acquired waveform for best settings is reported.

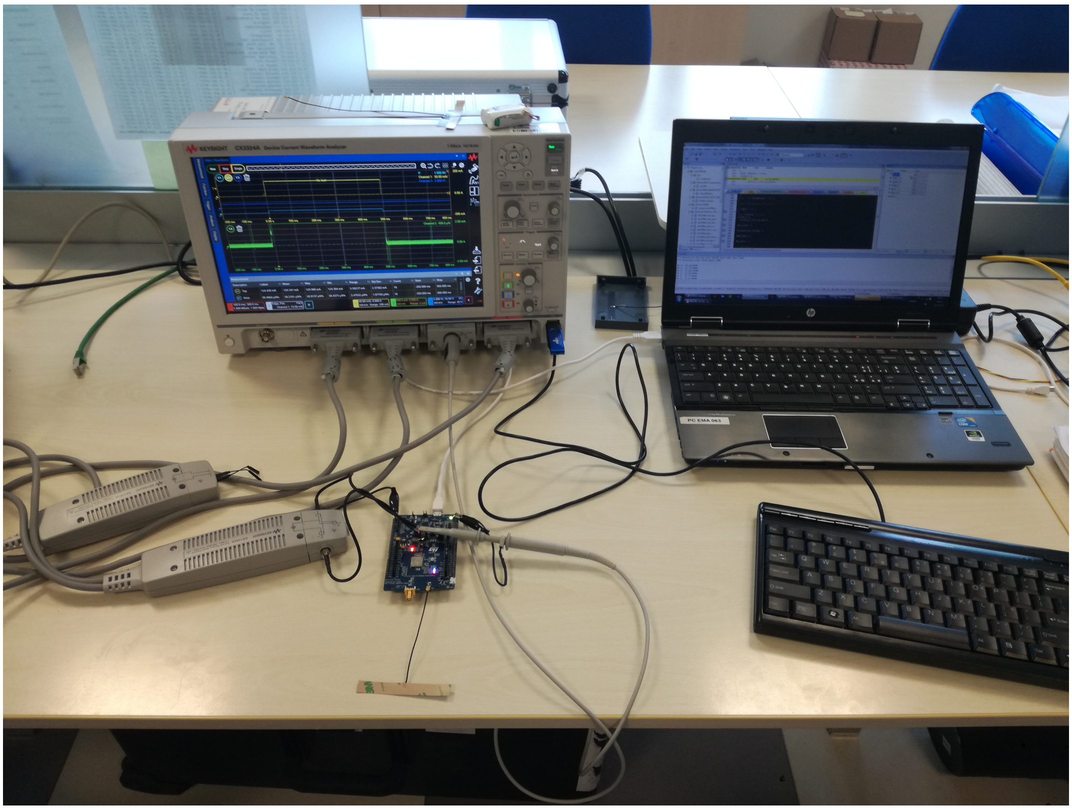

Figure 3.10. Measurements set-up.

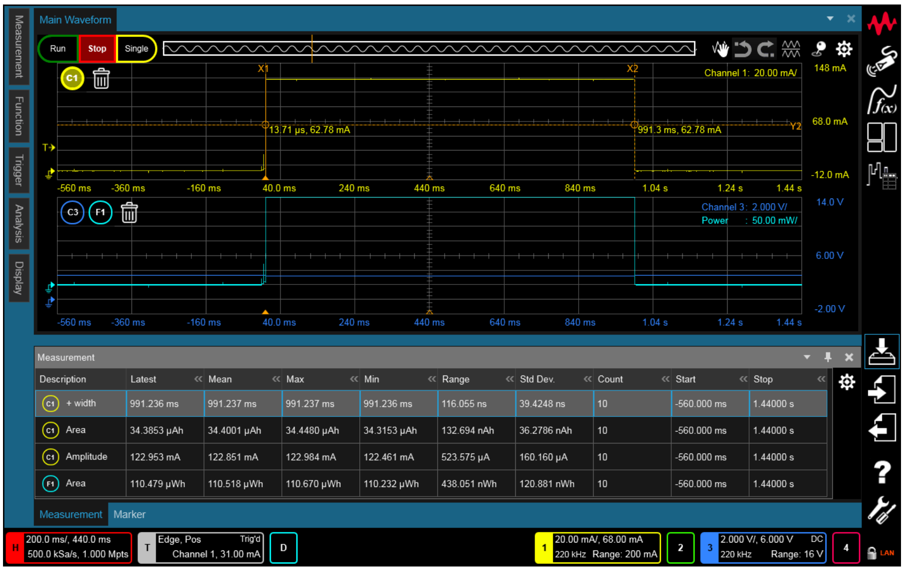

Figure 3.11. Acquired waveform with a $SF = 12$, $BW = 125$ kHz and 20 dBm$of output power$.

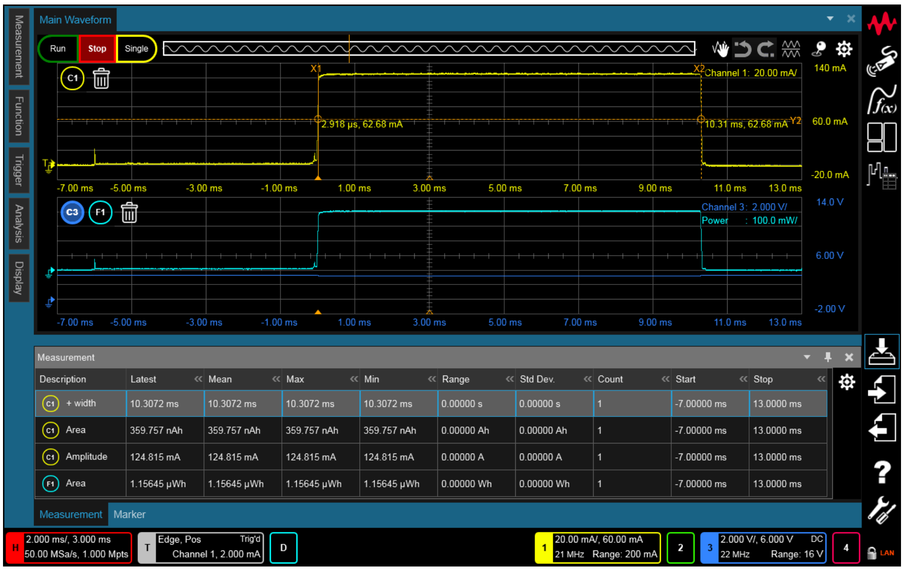

Figure 3.12. Acquired waveform with a $SF = 7$, $BW = 500$ kHz and 20 dBm$of output power$.

In Table 3.5, 3.6, 3.7, 3.8, 3.9, 3.10 and 3.11 the maximum current are reported, as well as power and energy for every transmissions with different values of bandwidth and power.

SF	Current [mA]	Energy [μWh]	Charge [μAh]	Duration [s]	Expected [s]
12	122.9	110.5	34.4	991.237	991.23
11	122.7	65.5	19.8	577.538	577.54
10	122.6	33.1	9.9	288.768	288.77
9	123.0	16.8	5.1	144.383	144.38
8	124.0	8.7	2.6	72.193	72.19
7	121.8	4.6	1.4	41.214	41.22

Table 3.5. Measurements for different spreading factor with $PWR_{out} = 20\,\mathrm{dBm}$, and $BW = 125\,\mathrm{kHz}$.

SF	Current [mA]	Energy [μWh]	Charge [μAh]	Duration [s]	Expected [s]
12	123.5	54.1	16.8	495.620	495.62
11	123.1	27.0	8.6	247.811	288.77
10	123.0	15.7	4.8	144.390	144.38
9	123.4	8.0	2.5	72.197	72.19
8	124.2	4.3	1.3	36.098	36.10
7	122.8	2.4	0.8	20.610	20.61

Table 3.6. Measurements for different spreading factor with $PWR_{out} = 20\,\mathrm{dBm}$, and $BW = 250\,\mathrm{kHz}$.

SF	Current [mA]	Energy [μWh]	Charge [μAh]	Duration [s]	Expected [s]
12	87.2	88.2	27.3	991.234	991.23
11	86.7	51.4	15.9	577.536	577.54
10	89.0	25.9	8.1	288.766	288.77
9	85.5	12.8	4.0	144.385	144.38
8	86.9	6.6	2.1	72.191	72.19
7	87.5	3.8	1.2	41.213	41.22

Table 3.7. Measurements for different spreading factor with $PWR_{out} = 17\,\text{dBm}$, and $BW = 125\,\text{kHz}$.

SF	Current [mA]	Energy [μWh]	Charge [μAh]	Duration [s]	Expected [s]
12	87.2	44.3	13.8	495.618	495.62
11	86.7	22.2	6.9	247.809	288.77
10	89.0	12.7	3.9	144.387	144.38
9	85.5	7.0	2.1	72.195	72.19
8	86.9	3.7	1.1	36.097	36.10
7	87.5	1.9	0.6	20.608	20.61

Table 3.8. Measurements for different spreading factor with $PWR_{out} = 17\,\text{dBm}$, and $BW = 250\,\text{kHz}$.

SF	Current [mA]	Energy [μWh]	Charge [μAh]	Duration [s]	Expected [s]
12	44.2	39.4	12.0	991.239	991.23
11	43.7	22.9	7.0	577.544	577.54
10	46.0	11.5	3.5	288.784	288.77
9	44.9	5.8	1.7	144.400	144.38
8	44.1	2.9	0.9	72.735	72.19
7	44.8	1.6	0.5	41.230	41.22

Table 3.9. Measurements for different spreading factor with $PWR_{out} = 14\,\text{dBm}$, and $BW = 125\,\text{kHz}$.

SF	Current [mA]	Energy [μWh]	Charge [μAh]	Duration [s]	Expected [s]
12	43.9	19.9	6.1	495.638	495.62
11	43.8	9.9	3.0	288.801	288.77
10	44.2	5.8	1.8	144.403	144.38
9	44.1	2.9	0.9	72.208	72.19
8	44.0	1.5	0.5	36.116	41.22
7	43.9	0.8	0.3	20.627	20.61

Table 3.10. Measurements for different spreading factor with $PWR_{out} = 14\,\text{dBm}$, and $BW = 250\,\text{kHz}$.

SF	Current [mA]	Energy [μWh]	Charge [μAh]	Duration [s]	Expected [s]
12	44.2	10.0	3.1	247.832	247.81
11	43.3	4.9	1.5	123.927	144.38
10	44.2	2.8	0.86	72.215	72.19
9	43.9	1.5	0.45	36.119	36.1
8	44.0	0.74	0.23	18.070	18.05
7	44.0	0.42	0.13	10.327	10.3

Table 3.11. Measurements for different spreading factor with $PWR_{out} = 14\,\text{dBm}$, and $BW = 500\,\text{kHz}$.

Chapter 4

Model development and analysis

4.1 Battery choice and management

The battery chosen to power the sensor is a lithium thionyl chloride ($LiSOCL_2$). The choice was made after a depth study on different batteries available on the market. As previously said, the meter shall not require any intervention from the final user and for this reason a primary (non rechargeable) lithium battery has been chosen; lithium primary batteries have a very high capacity compared with *li-ion* rechargeable batteries. Moreover, the $LiSOCL_2$ in particular have by far the best charge weight ratio.

The actual used battery is a pack composed of two SAFT *LS17500*[20], characterized by an Open Circuit Voltage (OCV) of 3.6 V and a capacity of 3600 mAh, mounted in parallel in order to provide 7200 mAh in total. In our case, the charge weight ratio is approximately

$$C/W_{ratio} = \frac{3.6\,\mathrm{V} \cdot 3.6\,\mathrm{Ah}}{20.9\,\mathrm{g}} \approx 600\,\mathrm{Wh/kg}$$

This battery is characterized by a very flat discharge curve, a typical discharge profile, for different discharge currents, is reported in Figure 4.1.

Due to this characteristic, the estimation of the residual charge of the battery is very complicated. In order to address this necessity, the a study has been conduced on this topic.

There are few available systems on the market that could make some prevision on the state of charge of this type of batteries. The most promising was the BQ35100: this IC is produced by Texas Instrument precisely in order to work with $LiSOCl_2$ battery (and also with $LiMnO_2$)[21].

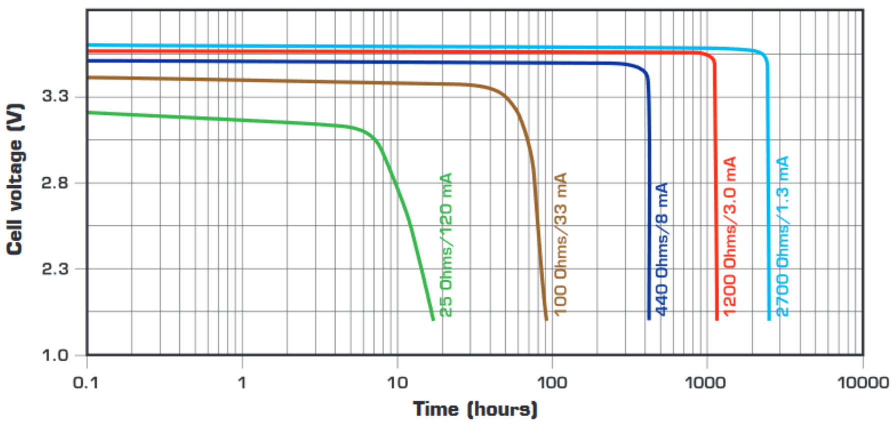

Figure 4.1. Discharge characteristic of $LiSOCL_2$ LS17500 battery.

This IC could work in three different mode[22]:

- Accumulation mode (ACC): in this configuration the sensor measures all the charge that flow through its shunt resistor[1]. The IC executes a continuous multiplication between current and voltage to compute the charge extracted from the battery, this is typically refereed as *coulomb counter*. The sampling time is 8 ms.
- End of Service mode (EOS): this mode is intended to be used with $LiMnO_2$ batteries, and is not applicable to our system, in any case this mode determines the charge state doing a correlation between OCV and temperature;
- State of Health mode (SOH): this configuration is fitted to estimate the residual charge in the $LiSOCl_2$ batteries. In this mode a TI proprietary algorithm correlates current, voltage and temperature in order to estimate the internal impedance of the cell and then return the state of charge of the battery.

4.1.1 BQ35100 results

In order to test the functionality and verify the correct behavior, different tests was conducted on the $BQ35100$, using an evaluation board and the USB-I^{2}C interfaces *EV2300*, both produced by TI. The setup is shown in Figure 4.2.

[1] A shunt resistor has, typically, a low and precise value and it is used to give a stable voltage drop when current flow through it.

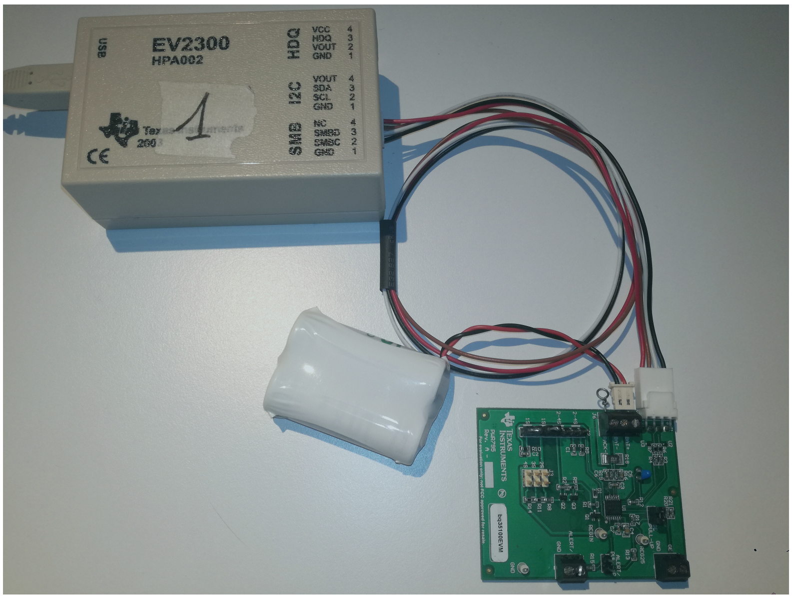

Figure 4.2. Test setup for $BQ35100$.

The flat discharge profile of the battery was a problem from the beginning. In fact, the EOS mode turned out to be difficult to implement. The computed impedance of the algorithm was very dependent by the type, the duration and amplitude of the load current.

For example with an electronic load the result was reliable and repeatable, instead using the radio module as load, the result was very unpredictable and highly dependent on the LoRa parameters settings.

For these reasons, the accumulator (ACC) mode was choices, the problem in this mode are that, as all the *coulomb counter*, there is a drift error due to not ideal calibration that could be significant, the calibration procedure is related to the board (PCB traces, shunt resistor tolerance, ecc.) and is difficult guarantee an adequate repeatability for series production.

For example, supposing a 1 µA incorrectly measured every 100 s lead to an *apparent* mean current of

$$\Delta I_{mean} = 1\,\mu\text{Ah} \cdot \frac{3600\,\text{s/h}}{100\,\text{s}} = 36\,\mu\text{A}$$

and after one year the error of the measured charge could be

$$\Delta C_{year} = 36\,\mu\text{A} \cdot 24 \cdot 365 \approx 316\,\text{mAh}$$

that is approximately the 5% of the total charge of the battery.

Due to the unreliability of the EOS mode was chosen the ACC solution, even if this mode is affected by some estimation errors, it can guarantee a better accuracy about the battery charge state.

C library has been developed in order to control the gauge by Micro Controller Unit (MCU), the library is reported in Appendix A.

4.2 Data input acquisition

An acquisition system has been developed to acquire some real data to use with the model. This was implemented using a commercial board, the *STM32F4DISCOVERY* designed by *STMicroelectronics*.

The system is shown in Figure 4.3: it is composed by the STM32F4DISCOVERY board, an USB adapter that allows the use of a classical USB drive, a small circuit used only to maintain the system on, an USB power bank and an additional board with a comparator and a photodiode that is coupled with a Plastical Optical Fiber (POF) that is used to capture the power meter blink.

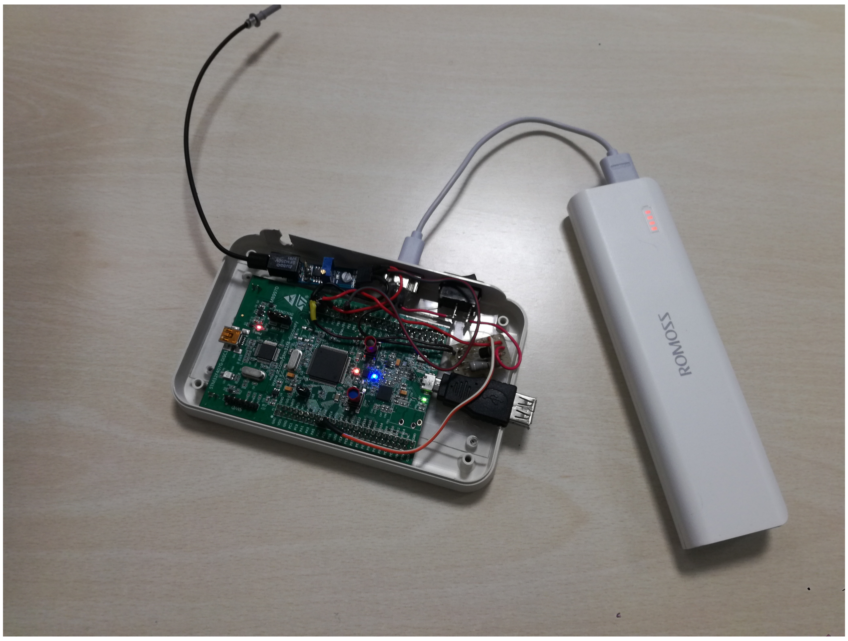

Figure 4.3. Data acquisition system.

The installation on the power meter is shown in Figure 4.4

This data-logger is intended to acquire the time elapsed between the blinks of the power meter. The acquired time is expressed in *ms*.

The actual used power is computed considering that standard power meters

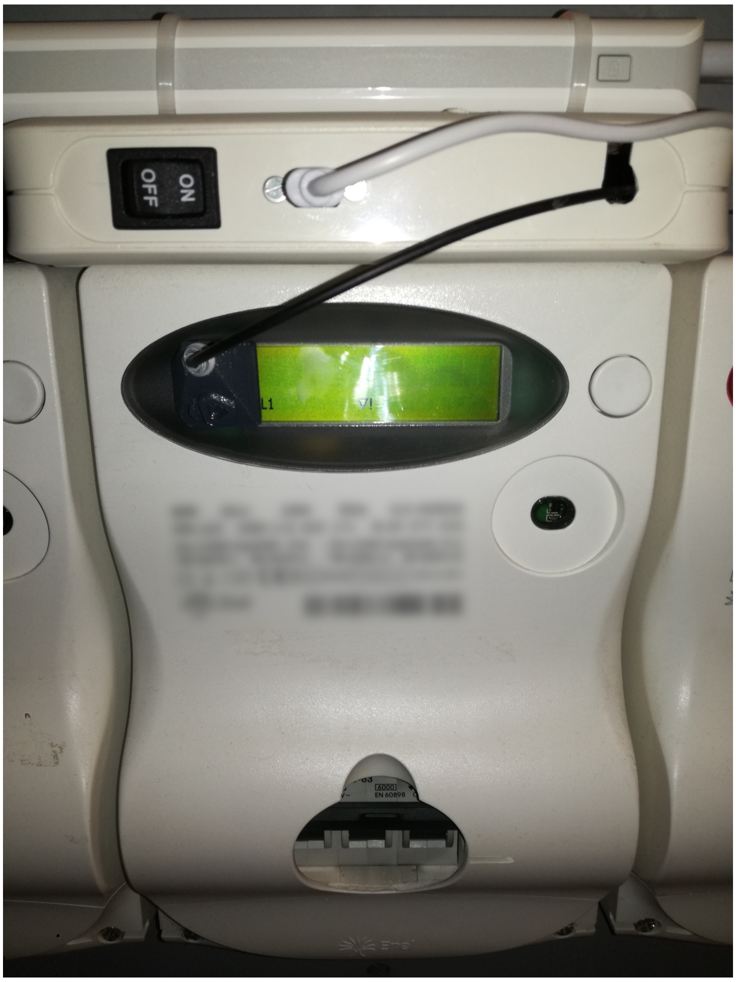

Figure 4.4. Data acquisition system mounted on the power meter.

have a characteristic of 1000 $imp/kWh = 1\ imp/Wh$ and then power can be obtained as reported in Eq. 4.1.

$$P = \frac{3600\,\mathrm{s/h}}{1\,\mathrm{Wh}^{-1} \cdot t_{ms} \cdot 1000} \tag{4.1}$$

A typical output of the acquisition is shown in Figure 4.5. This profile is related to domestic environment and is an extract of a longer acquisition. The spike corresponds to an oven ignition, the periodic rectangular profile are related to the refrigerator compressor activation. The acquisition lasts for 15 hours, and proximately in the middle there is the transition to the night-time, where the used mean power is smaller, and only the refrigerator contribution remains active.

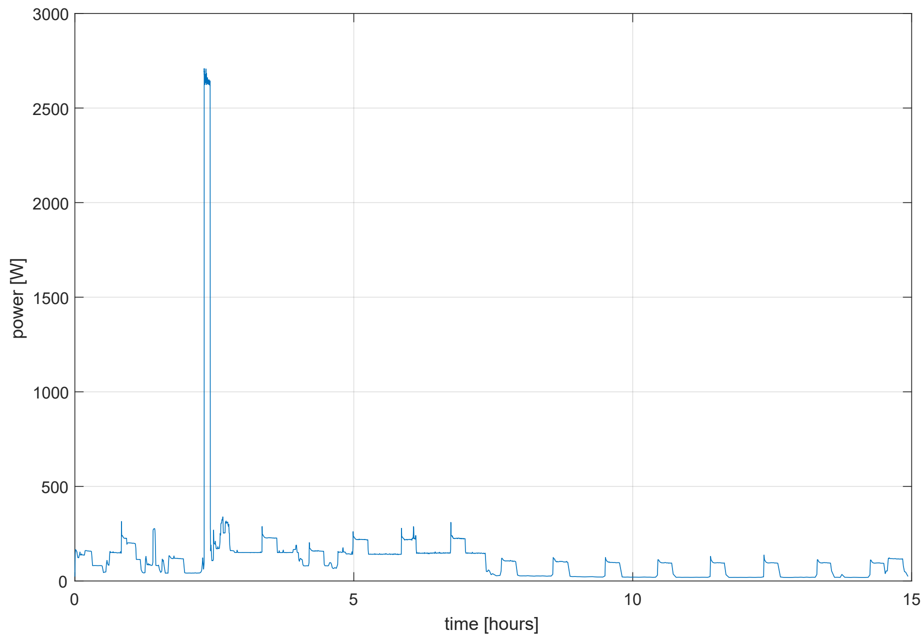

Figure 4.5. 15 hours of domestic profile acquisition.

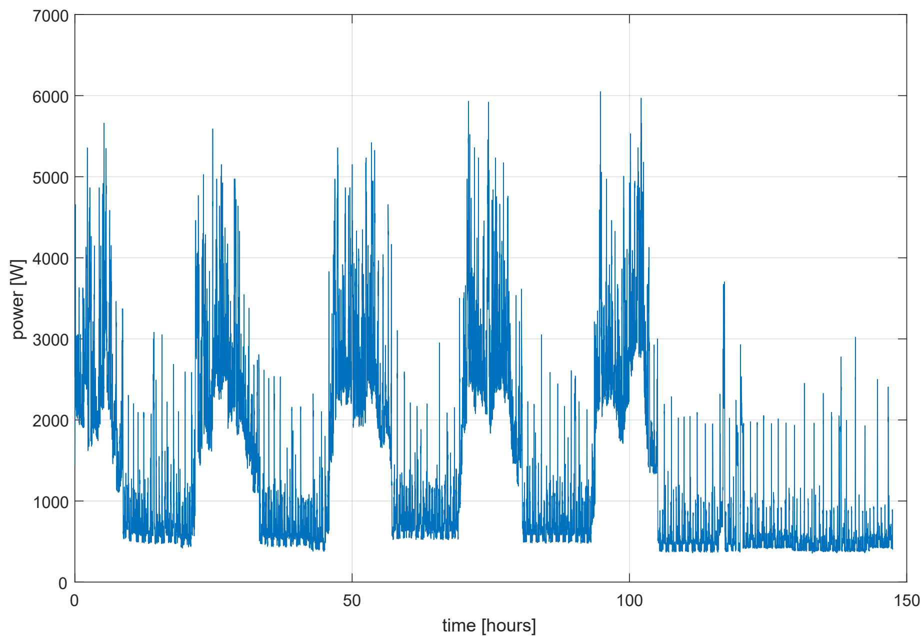

Figure 4.6. 6 days small office profile acquisition.

4.3 Protocol implementation

The message is composed by 13 bytes. This dimension was chosen to match some requirements; the first is to guarantee a time of 100 seconds between two consecutive messages, in the worst case of radio settings, or rather with spreading factor equal to 12 and a bandwidth of 125 kHz; the second is the dimension of the packet itself that must be greater than 8 bytes in order to contain all the useful information for the implemented P2P protocol. A non-fixed message type has been discarded in order to have a predictable behaviour in term of channel occupation, energy consumption and reliable simulation results.

The choice of the length of the message could be better explained using some formulas.

For different configurations could be esteemed the energy used to transmit every byte. Firstly, the used energy to transmit the entire message is computed as reported in Eq. 4.2.

$$E_{msg} = I_{RF} \cdot t_{TX} \tag{4.2}$$

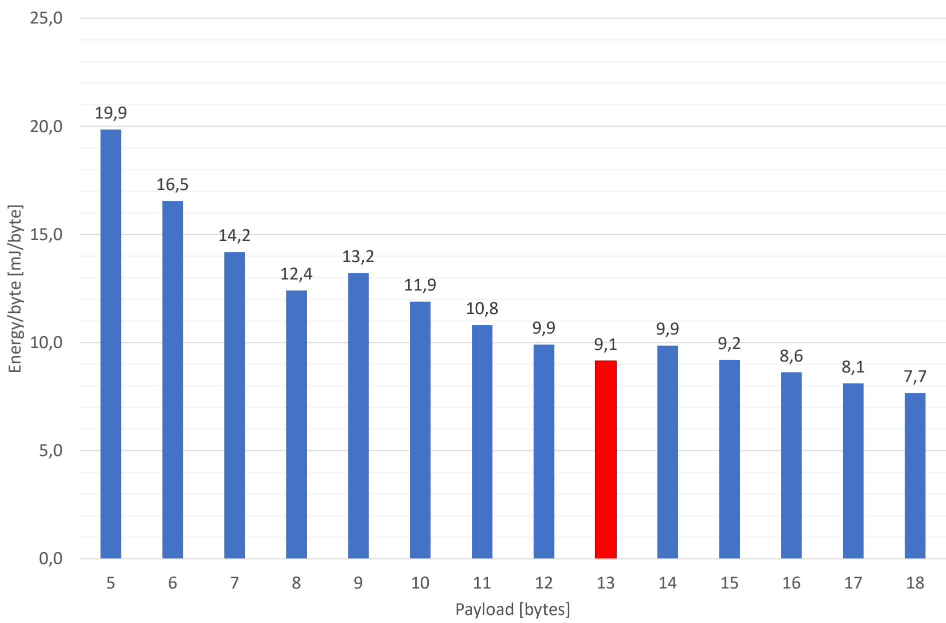

Figure 4.7. Energy per byte for different payload length.

Then, the energy used for a transmission of a single byte could be computed as expressed in Eq.4.3.

$$E_{tx_{byte}} = \frac{E_{msg}}{n_{payload}} \text{ [mJ/byte]} \tag{4.3}$$

In Figure 4.7 are reported the results considering an output power of 20 dBm, with a current consumption of 20 mA, and a preamble of 8 symbols. It can be seen that the selected configuration could guarantee a ratio of 9.1 mJ/byte, this value could be improved using a bigger payload, but with an increasing of the transmission time and a overall energy consumption.

The message are sent without any type of acknowledge from the gateway except for some messages sent every 900 s. This is the main difference with LoRaWAN, in fact every receiving windows prescribed by the protocol represent an energy consumption.

The absence of acknowledges implies also the impossibility of using re-transmissions in case of packet lost, that could be unusual in case of massive presence of concrete and obstacle.

Only one special message requires an ACK because its content is more important for the customer. Moreover, as for LoRaWAN, during the receiving window of the sensor, the gateway, along with the ACK, send also eventual new settings.

Two time window could be defined, the main window, which lasts for 900 seconds (15 minutes, is a fixed value) and the sub-window that has a variable duration but with fixed steps (2", 3", 6", 9", 10", 18", 30", 60", 75", 100", 150", 180", 225", 300").

A schematic representation is reported in figure 4.8.

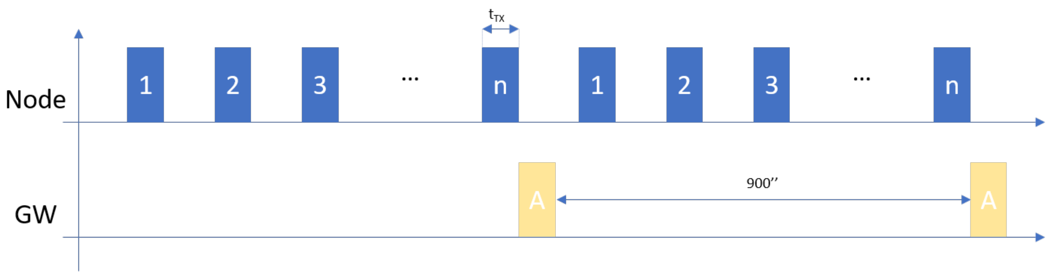

Figure 4.8. Graphical representation of custom protocol.

4.4 Blinks acquisition consumptions considerations

The blinking of the meter LED is acquired by means of a photodiode and sampled by the MCU. The LED light is driven to the photodiode through a light guide of about 3 cm length. The LED blinking is characterized by 10 ms T-on, this time was obtained by measuring on different meters with different supply limit, and a variable frequency from 0.833 Hz (1200 s) to 12.5 Hz (80 ms), calculated from the limit at lower (one blink each 20 minutes) and higher consumption ($P_{max-x} = 45\,000\,\text{kW} \cdot 1.25$) considering the typical unit of 1 impulse/Wh.

Light detection can be influenced by an external light that can filters from the meter display. So the circuitry is properly designed to not be sensitive to this noise.

Two software solution could be implemented to acquire the blink:

- using a low-energy counter that can operate without the CPU supervision and is checked every predefined time window. The drawback is that only at the end of time window the power could be estimated without the possibility of monitoring the instantaneous power.

- using an interrupt triggered by the blink, in the ISR the total counter is incremented; the main advantage of this solution is that the delta time between each blink could be acquired and then is possible to monitoring also the instantaneous power.

The energy consumption of these strategies is comparable if the blink frequency is low (e.g. domestic environment), but for high frequency (e.g. industrial environment), from the energy point of view, the second solution is better but losing the possibility to detect power peak.

Two different strategies are shown in Figure 4.9, with a) is indicated the first solution and with b) the second one.

The actual implementation adopts the second solution to be able to provide a more precise result.

4.5 Power amplifiers efficiency and output power

Other considerations was done on the RF part of the system. Inside the *SX1276* there are three PAs, one of them is not usable at our frequencies, the other two differs on the efficiency and and maximum power output. The low power one can provide an output power up to $+14dBm$, the other can provide a power of $+20dBm$. To maximize the link budget also this PA is exploited.

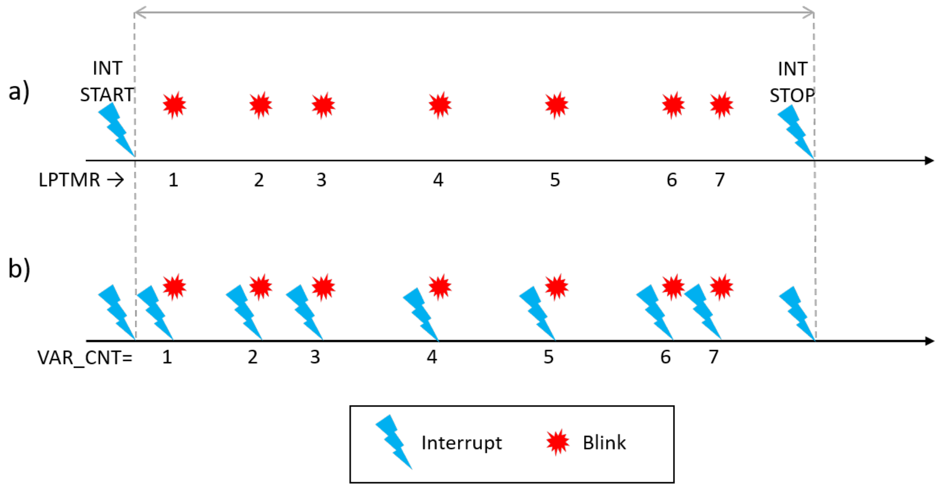

Figure 4.9. Different blinks acquiring method.

The limits of the ETSI regulations are referred to ERP. Power at the pin of the transceiver could reach $+20dBm$, but a poor matching network and a low efficiency antenna (an adhesive antenna has been used) provide about $+14dBm$ ERP. In future development, in which the matching network will accurate tuned and a better antenna will be designed, the output power must be keep low in order to be compliant with the ETSI specific.

The efficiency of the PAs could be computed as follow

$$\eta_{PA} = \frac{P_{DC}}{P_{RF}} \tag{4.4}$$

It was soon noted that the output current is strongly dependent on the length of the antenna cable; three different length has been tested: 10 cm, 15 cm and 20 cm. The three different antenna are shown in Figure 4.11.

The current measures (without the current contribution due to TCXO, that is about 1.6 mA) are reported in Table 4.1.

Cable length $[cm]$	Mean current $[mA]$
10	121
15	113
20	130

Table 4.1. Current measurements for different coaxial cable lenght.

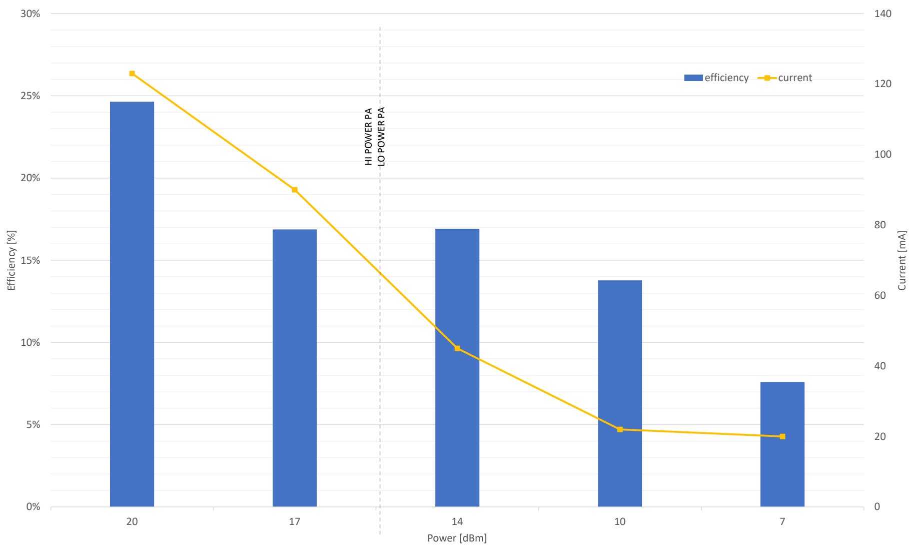

Figure 4.10. PAs efficiency and current consumption.

Figure 4.11. 10 cm, 15 cm and 20 cm antenna coaxial cable configuration.

The different currents can be explained by the fact that the variation of the cable length causes a variation of the reflected power and, therefore, and increasing or decreasing of the current. The optimal length choice is 10 cm, in fact with this length the current (without the current contribution due to the TCXO) is comparable to that indicated in the datasheet (120 mA) and, therefore, could be assumed that guarantee a better matching.

4.6 Model overview

The main goal of the project is to estimate the power consumption of the device in order to forecast the battery life of the sensor and a design a sort of strategy to decrease the energy consumption.

The main contribution to battery discharge is to be attributed to transmissions, but a primary goal is to obtain a real-time information, therefore, an high number of transmission are required.

A fundamental issue is the message dimension; a commercial solution, as already mentioned, was discarded because of the overheads and inefficiencies due to be compatible in several scenarios. This obliged to design a custom protocol as much as possible tailored for the application.

The model was first implemented with Matlab and Simulink; the performance of the simulation was slow since that the simulation period, in some case, was very long.

To guarantee a faster execution, the model was implemented in *SystemC*, this is a C libraries set that provide a discrete-event simulation environment and allows the execution of concurrent process.

The used language was C++, this is motivated also by the fact that in this way it was possible to simulate directly the FW code of the MCU to test it and verify the correct behavior and evaluate in a very fast way how the changes impact on the energy performances.

The model simulation setup is shown in Figure 4.12.

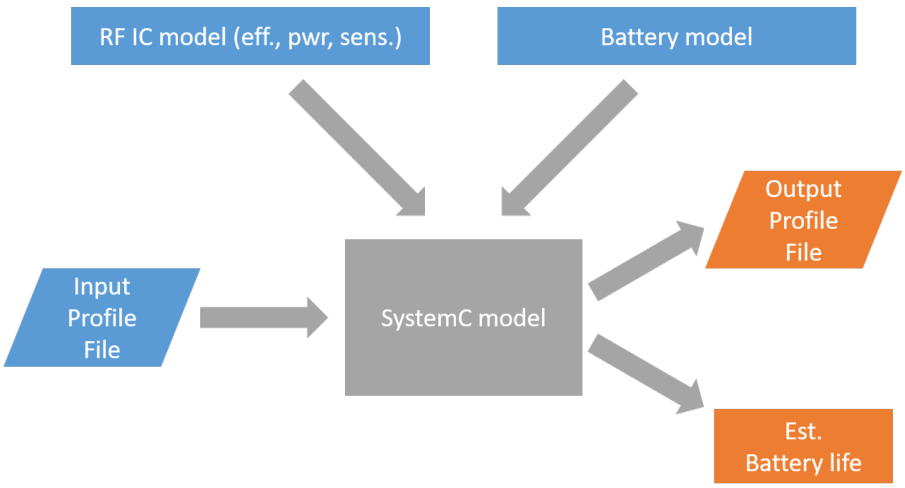

Figure 4.12. Schematic setup of simulation.

4.6.1 Update strategy

A custom strategy for the transmission of the consumption data has been studied to achieve the best battery usage and allow a high transmission rate compliant with ETSI regulation.

At the end of the main window the message is always sent, this is indicated in Figure 4.8 with message n. Every sub-window the power could be sent or not (messages indicated with numbers in Figure 4.8); the decision to transmit or not this data is made considering the value of the previous sent power, if the new value departs from the previous one of a threshold value, set by the cloud, the new power is sent otherwise not (in any case the power is sent for three times also if the power doesn't change, for guarantee the correct delivery of the data); there are two thresholds, one for the rising and one for the falling phases, the transmission policy is shown in Figure 4.13.

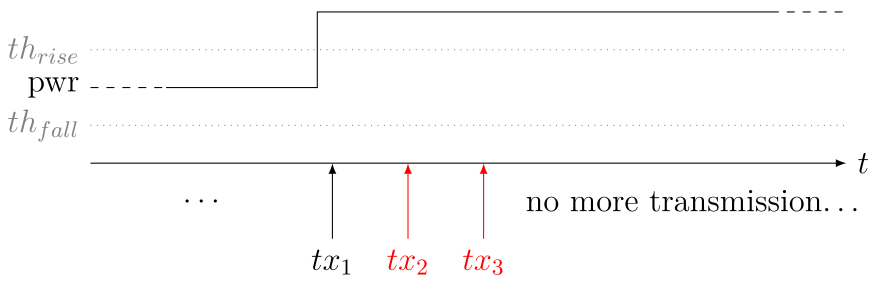

Figure 4.13. Transmission policy.

The power is evaluated in a temporal window, this imply that the power cannot be represented in a real-time view, but to decreasing the time window a very fast response could be obtained.

There are two different power estimation method, one is based on the mean power over the sub-window, the other one is the instantaneous power computed every blink in the ISR. To represent the power in the best possible way a weighted average of these two value is evaluated, the choice of the weight factor *alpha* could be done in a dynamic way; in Figure 4.14 is graphically represented the power estimation based on the value of *alpha*.

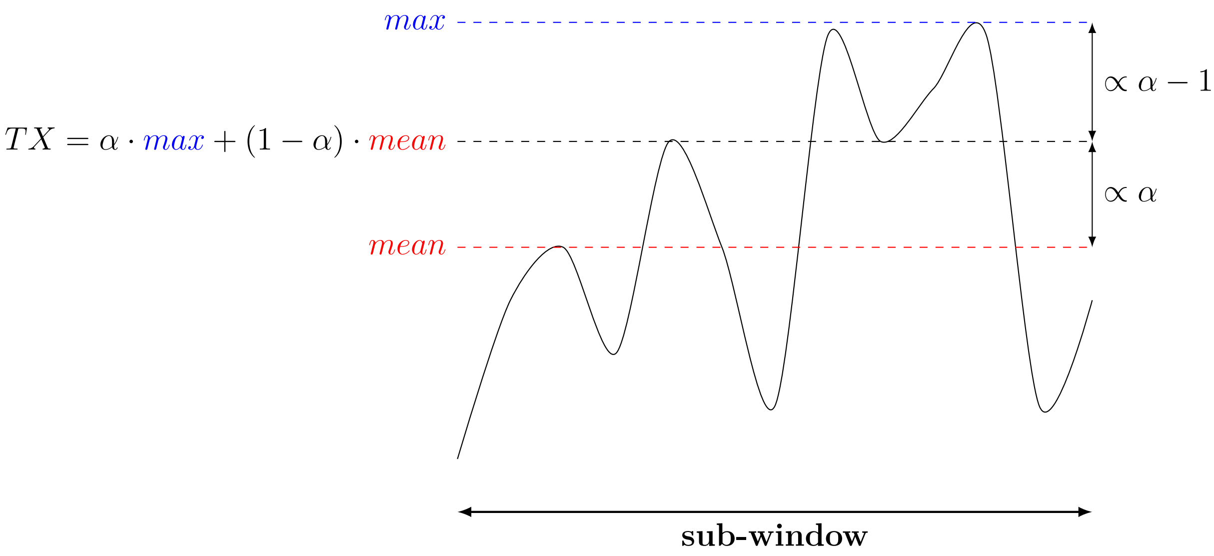

Figure 4.14. Hybrid power estimation.

4.6.2 Model implementation

An accurate representation of the model could be seen in Figure 4.15.

The input are:

- A dummy o an acquired power profile to emulate the signal acquisition;
- the characteristics of the battery (that in the default case are: $3.6V$, $7200mAh$ and a self discharge of $2\%/year$);
- the LoRa parameters.

The output are:

- Output profile elaborated by the DUT;
- Estimation of consumed energy, number of transmissions, the time spent by the MCU in sleep, idle or run state.

From the input LoRa parameters, the transmission time, the minimum time between two consecutive transmission, the withdrawn of each of them and the link budget are avaluated.

In the SystemC model the input file is acquired, this is passed to the meter in order to simulate a real application. This input is elaborated by the sensor and the eventual transmission is simulated

At every transmission an amount of charge is removed from the battery, this quantity is that was computed in the previous chapter. The battery discharge is influenced also by the current absorbed by the MCU, which depends on its operating state (sleep, idle or run) and also on the self discharge rate of the battery itself.

To simulate the radio channel a `sc_module` has been used. This model has been useful also to evaluate how many collisions could appear when there are many nodes that share the same area. This aspect will be investigated in future developments to improve the quality of the prediction, that will be based also on the distance of the nodes and the signal strength.

The input and output file are directly plotted by the program itself using gnuplot[23]; this is a open-source software controlled by a command line interface, that, in this case, is managed by the program.

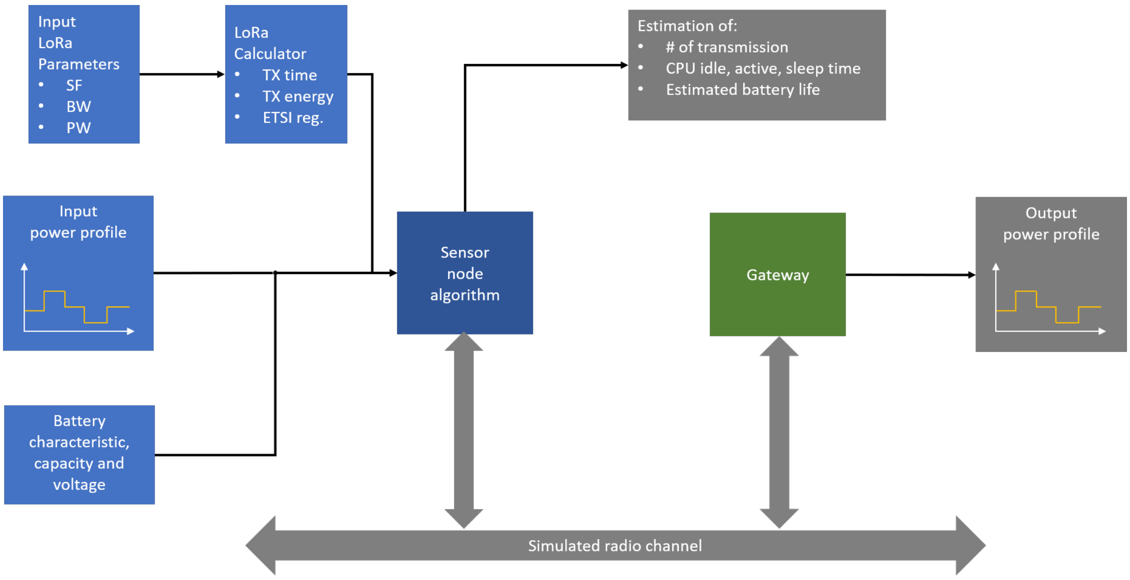

Figure 4.15. Schematic setup of simulation.

Chapter 5

Results

A typical results window, returned by the simulator, is shown in Figure 5.1, the returned output are:

- the number of packet collision on the radio channel (that in this case is 0 because of the presence of only one sensor);
- the MCU statistics;
- the energy consumed during the simulation;
- and the estimated battery life.

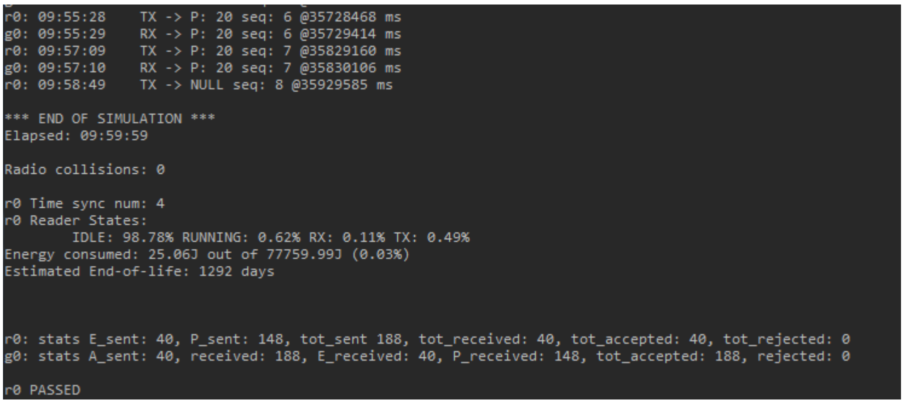

Figure 5.1. Typical output window.

To show the influence of the radio parameters two results are reported in Figure 5.2 and 5.3. In the first case a sub window of 100 s was chosen, instead in the second case the adopted window is 10 s. The input file is the same used in Figure 4.5.

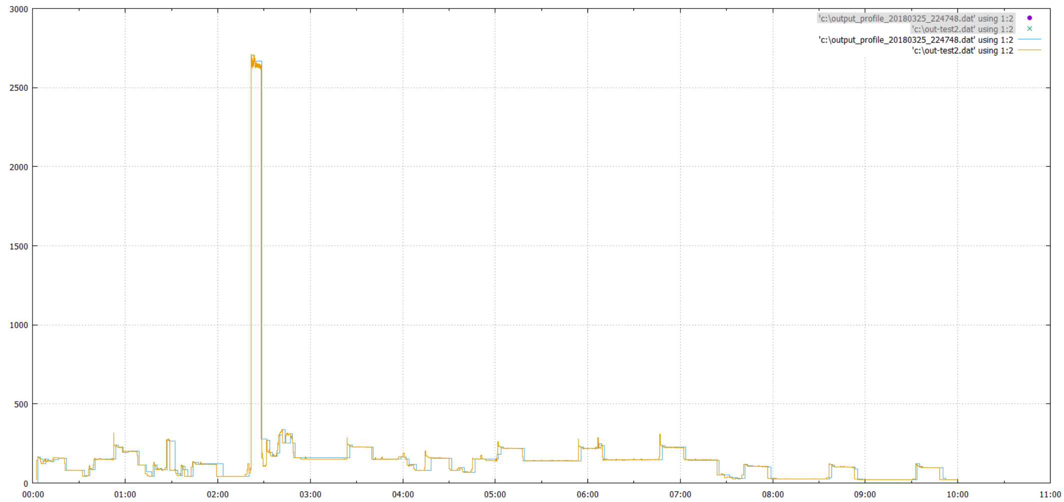

Figure 5.2. Output profile with 100 s of time window.

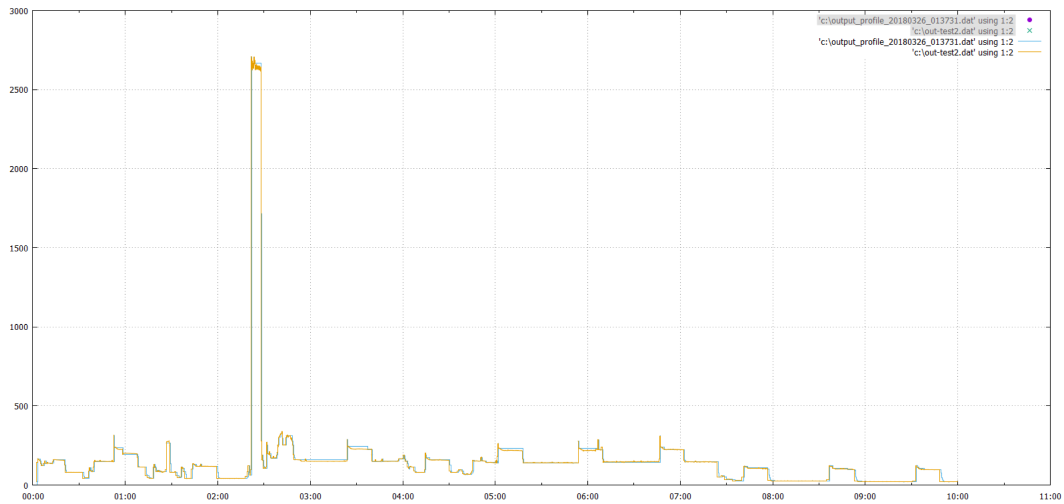

Figure 5.3. Output profile with 10 s of time window.

It can be seen how, in the second plot, the power profile is better approximated by the sensor, and the temporal resolution has improved.

Without any strategy implementation the battery life of the sensor would be less than 3 years in any case as Table 5.1 shows; thanks to this study it was detected a strategy that made possible to reach a battery life of about 3 years. This model is important to evaluate how a change in the code of the sensor or in the strategy algorithm impact on the battery discharge, that otherwise would require long test procedures.

SF	BW [Hz]	Tsym [ms]	Tonair [ms]	WIN min [s]	WIN [s]	Life [days]	Life w/ strat.[days]
6	125.0E+3	0.51	23.2	2.3	3	307	1589
7	125.0E+3	1.02	41.2	4.1	6	345	1433
8	125.0E+3	2.05	72.2	7.1	9	295	1326
9	125.0E+3	4.10	144.4	14.3	18	295	1298
10	125.0E+3	8.19	288.8	28.6	30	246	1256
11	125.0E+3	16.38	577.5	57.2	60	246	1232
12	125.0E+3	32.77	991.2	98.1	100	239	1196
6	250.0E+3	0.26	11.6	1.1	3	614	2340
7	250.0E+3	0.51	20.6	2.0	3	345	1601
8	250.0E+3	1.02	36.1	3.6	6	394	1402
9	250.0E+3	2.05	72.2	7.1	9	295	1390
10	250.0E+3	4.10	144.4	14.3	18	295	1324
11	250.0E+3	8.19	288.8	28.6	30	246	1298
12	250.0E+3	16.38	495.6	49.1	60	287	1243
6	500.0E+3	0.13	5.5	0.5	3	1284	1398
7	500.0E+3	0.26	10.3	1.0	3	690	1316
8	500.0E+3	0.51	18.0	1.8	3	394	1297
9	500.0E+3	1.02	36.1	3.6	6	394	1275
10	500.0E+3	2.05	72.2	7.1	9	295	1247
11	500.0E+3	4.10	144.4	14.3	18	295	1389
12	500.0E+3	8.19	247.8	24.5	30	287	1302

Table 5.1. Estimated battery life without any strategy.

Chapter 6

Conclusion and future developments

In order to improve the system two ways could be followed; the first way is improve the prediction process and therefore the SystemC model, the simulation of the radio channel model could be modified to represent in a more realistic way its behaviour, and take into account also the collisions based on the RSSI value and spatial distribution of the nodes of the network.

Another way to improve the system may be a more depth study of the antenna and its efficiency, to avoid wasting energy due to a non optimized antenna. And a complete redesign of the RF front, such as the matching network, and the power amplifier.

For the latter matter a possible solution is the adoption of the new Semtech's IC family, *SX126x*, that lead to an improvement of the efficiency of the power amplifier, this could be seen from Figure 6.1[19], this IC is able to provide an output power of 22 dBm with the same current used by the actual IC, thus been able to guarantee and efficiency of about 40%.

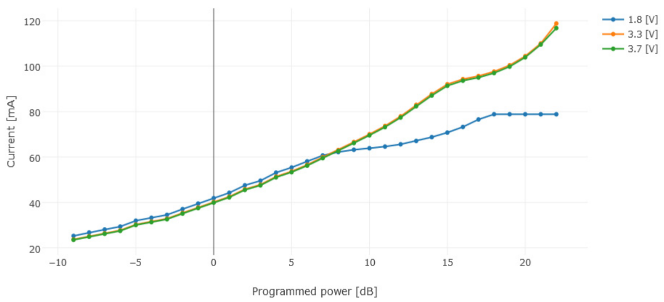

Figure 6.1. Current consumption versus RF output power of SX1262.

Another way to increase the efficiency an external PA could be used. A possible solution could be the adoption of a PA designed by *SKYWORKS*, the *SKY66420*, considering the specific reported on the datasheet, can be estimated an efficiency of about 54%.

Bibliography

[1] M. Centenaro et al. *Long-Range Communications in Unlicensed Bands: the Rising Stars in the IoT and Smart City Scenarios*. Vol. 23. 2016.

[2] IEEE Computer Society. *802.15.4, Part 15.4: Wireless Medium Access Control (MAC) and Physical Layer (PHY) Specifications for Low-Rate Wireless Personal Area Networks (LR-WPANs)*. 2003.

[3] ZigBee Alliance. *ZigBee Specification*. 2012.

[4] K. Li G. Shi. *Fundamentals of ZigBee and WiFi*. 1st. Prentice Hall Professional Technical Reference, 2016.

[5] I. Unwala and J. Lu. *IoT Protocols : Z-Wave and Thread*. Vol. 3. 2017.

[6] Inc. Thread Group. URL: https://www.threadgroup.org/.

[7] Inc. Thread Group. *Thread 1.1.1 Specification*. 2017.

[8] LitePoint. *Bluetooth Low Energy Whitepaper*. 2016.

[9] DASH7 Alliance. URL: http://www.dash7-alliance.org/.

[10] Jean-Marie Gorce Claire Goursaud. *Dedicated networks for IoT : PHY / MAC state of the art and challenges*. 2015.

[11] LoRa Alliance. *A technical overview of LoRa and LoRaWAN*. 2015. URL: https://www.semtech.com/uploads/documents/an1200.22.pdf.

[12] Andrew S. Tanenbaum and David J. Wetherall. *Computer Networks*. 5th. Prentice Hall Professional Technical Reference, 2011.

[13] Sakshama Ghoslya. URL: http://www.sghoslya.com/p/lora_6.html.

[14] LoRa Alliance. *LoRaWAN 1.1 Specification*. 2017.

[15] Thomas Clausen Augustin Aloys Jiazi Yi and William M. Townsley. *A Study of LoRa: Long Range and Low Power Networks for the Internet of Things*. 9. 2016.

[16] Semtech. *AN 1200.10 ETSI Compliance of the SX1272/3 LoRa Modem*. 2013.

[17] Semtech. *AN1200.22 LoRa Modulation Basics*. 2015. URL: https://www.semtech.com/uploads/documents/an1200.22.pdf.

[18] William H. Tranter Rodger E. Ziemer. *Principles of Communications: Systems, Modulation and Noise*. 7th. Wiley, 2014.

[19] Semtech. *SX1261/2 Datasheet*. 2018.

[20] SAFT. *LS17500 Primary lithium battery datasheet*. 2008.

[21] Texas Instruments. *bq35100 Lithium Primary Battery Fuel Gauge and End-Of-Service Monitor*. 2016.

[22] Texas Instruments. *bq35100 Technical Reference Manual*. 2016.

[23] GNUplot website. URL: http://http://www.gnuplot.info/.

[24] Semtech. *AN1200.13 SX1272/3/6/7/8: LoRa Modem Designer's Guide*. 2013.

[25] N. Benvenuto and M. Zorzi. *Principles of Communications: Systems, Modulation and Noise*. 1st. Wiley, 2011.

[26] V. K. Verma M. Arsalan A. Umair. *Dash7: Performance*. Vol. 2. 2012.

[27] CEPT. *ERC 70-03 Relating to the use of short range devices (SRD)*. 2015.

[28] ETSI. *ETSI EN 300 220-1, V2.4.1 "Electromagnetic compatibility and Radio spectrum Matters (ERM) Short Range Devices (SRD) Radio equipment to be used in the 25 MHz to 1 000 MHz frequency range with power levels ranging up to 500 mW"*. Part 1: Technical characteristics and test methods. 2012.

[29] D. Raddino J. Schlienz. *Narrowband Internet of Things Whitepaper*. 2017.

Appendix A

BQ35100 C library

```c
/*
 *  Alessandro Berruti
 *  17/10/17
 */
#include "bq35100.h"
#include "i2c_utils.h"

unsigned char gauge_start_cmd[] = {MAC_SUB_CMD, 0x11,0x00};
unsigned char gauge_stop_cmd[] = {MAC_SUB_CMD, 0x12,0x00};
unsigned char reset_cmd[] = {MAC_SUB_CMD, 0x41,0x00};
unsigned char new_battery_cmd[] = {MAC_SUB_CMD, 0x13,0xA6};
unsigned char status_subcmd[] = {MAC_SUB_CMD, 0x00,0x00};
unsigned char hw_type[] = {MAC_SUB_CMD, 0x03,0x00};

unsigned char i2c_data[4];

// return the internal temperature of bq35100
float temperature()
{
  I2C_Read_Reg( &hi2c1, GAUGE_ADDR, TEMP_REG, i2c_data, TEMP_LEN );
  float temperature_ret = ((i2c_data[1]<<8 | i2c_data[0]) - KELVIN_ZERO)/TEMP_DIV;
  Flush_Buffer(i2c_data,TEMP_LEN);
  return temperature_ret;
}

// return the charge provided by the battery (ACCUMULATION MODE)
long int charge()
{
  I2C_Read_Reg( &hi2c1, GAUGE_ADDR, CHARGE_REG, i2c_data, CHARGE_LEN );
  long int charge_t =  i2c_data[3]<<24 | i2c_data[2]<<16 | i2c_data[1]<<8 | i2c_data[0];
  Flush_Buffer(i2c_data,CHARGE_LEN);
  return (-charge_t);
}

// return the battery voltage (this parameter doesn't influences the the computation of the charge accumulation)
float voltage()
{
  I2C_Read_Reg( &hi2c1, GAUGE_ADDR, VOLTAGE_REG, i2c_data, VOLTAGE_LEN );
  int voltage = i2c_data[1]<<8 | i2c_data[0];
```

```c
  Flush_Buffer(i2c_data,VOLTAGE_LEN);
  return voltage/VOLT_DIV;
}

// return the state of health of the battery (SOH MODE)
char SOH()
{
  I2C_Read_Reg( &hi2c1, GAUGE_ADDR, SOH_REG, i2c_data, SOH_LEN );
  int SOH = i2c_data[1]<<8 | i2c_data[0];
  Flush_Buffer(i2c_data,SOH_LEN);
  return SOH;
}

// total capacity of the battery (cannot be changed)
short int totCapacity()
{
  I2C_Read_Reg( &hi2c1, GAUGE_ADDR, TOT_CAP_REG, i2c_data, TOT_CAP_LEN );
  int tot_cap = i2c_data[1]<<8 | i2c_data[0];
  Flush_Buffer(i2c_data,TOT_CAP_LEN);
  return tot_cap;
}

// start gauge
void gaugeStart()
{
  I2C_Write_Reg( &hi2c1, GAUGE_ADDR, gauge_start_cmd, MAC_SUBCMD_LEN );
}

// stop gauge
void gaugeStop()
{
  I2C_Write_Reg( &hi2c1, GAUGE_ADDR, gauge_stop_cmd, MAC_SUBCMD_LEN );
}

// reset gauge (doesn't reset the accumulated charge)
void bq35100Reset()
{
  I2C_Write_Reg( &hi2c1, GAUGE_ADDR, reset_cmd, MAC_SUBCMD_LEN );
}

// reset the accumulated charge or SOH
void newBattery()
{
  I2C_Write_Reg( &hi2c1, GAUGE_ADDR, new_battery_cmd, MAC_SUBCMD_LEN );
}

short int check_status()
{
  I2C_Write_Reg( &hi2c1, GAUGE_ADDR, status_subcmd, MAC_SUBCMD_LEN );
  I2C_Read_Reg( &hi2c1, GAUGE_ADDR, MAC_DATA_ADDR, i2c_data, MAC_SUBCMD_RESP_LEN
    );
  int status = i2c_data[1]<<8 | i2c_data[0];
  Flush_Buffer(i2c_data,MAC_SUBCMD_RESP_LEN);
  return status;
}

short int who_am_I_bq35100()
{
  I2C_Write_Reg( &hi2c1, GAUGE_ADDR, hw_type, MAC_SUBCMD_LEN );
  I2C_Read_Reg( &hi2c1, GAUGE_ADDR, MAC_DATA_ADDR, i2c_data, MAC_SUBCMD_RESP_LEN
    );
  int status = i2c_data[1]<<8 | i2c_data[0];
```

```
    Flush_Buffer(i2c_data,MAC_SUBCMD_RESP_LEN);
    return status;
}
```